Advancing chemical lability assessments of organic matter using a synthesis of FT-ICR MS data across diverse environments and experiments

Juliana D'Andrilli [a,*], Carlos M. Romero [b,1], Phoebe Zito [c], David C. Podgorski [c,d], Robert A. Payn [e], Stephen D. Sebestyen [f], Andrew R. Zimmerman [g], Fernando L. Rosario-Ortiz [h,i]

[a] Louisiana Universities Marine Consortium, Chauvin, LA 70344, USA
[b] Department of Chemistry and Biochemistry, University of Lethbridge, Lethbridge, Alberta T1K 3M4, Canada
[c] Department of Chemistry, Chemical Analysis & Mass Spectrometry Facility, University of New Orleans, New Orleans, LA 70148, USA
[d] Pontchartrain Institute for Environmental Sciences, Shea Penland Coastal Education and Research Facility, University of New Orleans, New Orleans, LA 70148, USA
[e] Department of Land Resources & Environmental Sciences, Montana State University, Bozeman, MT 59717, USA
[f] Northern Research Station, USDA Forest Service, Grand Rapids, MN 55744, USA
[g] Department of Geological Sciences, University of Florida, Gainesville, FL 32611, USA
[h] Department of Civil, Environmental, and Architectural Engineering, University of Colorado Boulder, CO 80309, USA
[i] Environmental Engineering Program, University of Colorado Boulder, CO 80309, USA

ARTICLE INFO

ABSTRACT

Patterns in Fourier transform ion cyclotron resonance mass spectrometry (FT-ICR MS) data provide perspective on how organic matter (OM) character is shaped by natural processes. Here, we reevaluate and update the molecular lability boundary (MLB) approach to assess OM lability using a synthesis of FT-ICR MS data. Now included are MLB_L (biolability) indices (i.e., the OM proportion of hydrogen-to-carbon ratios ≥ 1.5) of freshwaters, plant litter and biochar leachates, soils, and oils across the US, trends in OM and dissolved OM (DOM) lability from laboratory experiments examining isolated microbial, photochemical, and thermal degradation, and biogeochemical interpretations of biolability patterns across ecosystems influenced by human activity (e.g., fertilizer addition and agricultural management). Photo-processing increased the hydrogen saturation of OM, describing products of higher biolability ($>MLB_L$ values). DOM MLB_L values decreased during microbial and thermal degradation processes. Laboratory experiments with isolated treatments showed larger changes in MLB_L than exhibited by field samples from systems managed by humans. We interpret changes in N- and/or S-containing DOM above the MLB as the production or use of heterogeneously biolabile material. We interpret heterogeneously labile DOM composition to indicate autochthonous production, biomass growth, nutrient accumulation, or biological degradation in stream and soil samples. The most recent data in our synthesis suggest that the MLB approach should be reframed to provide lability indices for biotic, thermal, and photochemical processes. A broader perspective on lability provides a useful tool to decompose large, complex, and process-driven DOM data into more simple and informative indicators of trends in ecosystem form and function.

1. Introduction

The introduction of ultrahigh resolution Fourier transform ion cyclotron mass spectrometry (FT-ICR MS) at high magnetic field (greater than 7 T), first reported in Comisarow and Marshall (1974), has provided invaluable detailed molecular composition information to the organic geochemistry community. FT-ICR MS is used to characterize natural and engineered complex mixtures like dissolved organic matter (DOM) and petroleum (Hughey et al., 2002; Kujawinski et al., 2002; Stenson et al., 2003; Krajewski et al., 2017; Cooper et al., 2022). Over the last 20 years, researchers characterizing DOM composition using FT-ICR MS have introduced multiple metrics and approaches to simplify interpretation of the voluminous molecular data (Kim et al., 2003; Stenson et al., 2003; Hertkorn et al., 2006; Koch and Dittmar, 2006; Mopper et al., 2007; Purcell et al., 2007; D'Andrilli et al., 2013; D'Andrilli et al., 2015). Various methods have also been derived to highlight

changes in molecular composition driven by specific processes, extending understanding of system function at the molecular level (Kujawinski et al., 2004; Gonsior et al., 2009; Chipman et al., 2010; Stubbins et al., 2010; Podgorski et al., 2012; Minor et al., 2014; Ward et al., 2017; D'Andrilli et al., 2019; Zito et al., 2019; Wozniak et al., 2020). Organic matter (OM) and DOM transformations commonly assessed with FT-ICR MS analyses include: microbial heterotrophic degradation (Chipman et al., 2010; Logue et al., 2016; D'Andrilli et al., 2019; LaBrie et al., 2022; Wang et al., 2022), organomineral fractionation (Avneri-Katz et al., 2017; Coward et al., 2018), composting (Zhen et al., 2019), and photochemical degradation and dissolution (Kujawinski et al., 2004; Gonsior et al., 2009; Stubbins et al., 2010; Ray et al., 2014; Roebuck et al., 2017; Ward et al., 2017; Zito et al., 2019; Goranov et al., 2020; Zito et al., 2020). Most exploration of OM transformations using FT-ICR MS have been case studies of particular processes, and few studies have synthesized data representing diverse mechanisms of OM processing. We suggest that a more generalizable approach to deriving useful indices of OM reactivity and lability requires consideration of patterns in data from more diverse environmental systems or from experimentation with diverse environmental samples.

In 2015, D'Andrilli et al. proposed a molecular lability index using a threshold of the hydrogen-to-carbon ratio, where values of this ratio greater than or equal to 1.5 indicated notably more biolabile OM based on an extensive collection of FT-ICR MS DOM data generated from Alan G. Marshall's 9.4 T instrument at the National High Magnetic Field Laboratory (NHMFL), Tallahassee, Florida, USA. This molecular lability boundary (MLB) approach was designed to extend FT-ICR MS DOM interpretations of molecular data with respect to both compositional comparisons and patterns driven by natural processes (D'Andrilli et al., 2015). The index was derived from data synthesized over a decade (2005–2015) of FT-ICR MS analyses using samples from diverse ecosystems, which contributed to the potential generality of the approach. A major goal of that work was to develop a lability index from a relatively large and diverse DOM data set, allowing a broader interpretation of patterns in DOM FT-ICR MS data in the context of environmental carbon processing (D'Andrilli et al., 2015). The results showcased trends across ecosystems driven by the dominant source of carbon (allochthonous or autochthonous) in each reservoir. As DOM research using FT-ICR MS data continues to expand, further evolution of the logic developed in D'Andrilli et al. (2015) is needed to broaden perspective beyond the labile (MLB_L) and recalcitrant (MLB_R) categories (D'Andrilli et al., 2015).

A limitation of D'Andrilli et al. (2015) is that perspectives on lability were focused on soluble OM and included limited experimental manipulations. Here we use an extended data set adding more diverse analyses since 2015 to reevaluate the more general applicability of the MLB approach to characterize the potential modes of OM processing (D'Andrilli et al., 2015). We also include specific abiotic and biotic experimental manipulations to extend our understanding of DOM and OM cycling dynamics to accommodate additional mechanisms of chemical reactivity. To accomplish these goals, we conducted a synthesis, integrating a second decade of FT-ICR MS data from a diverse set of OM samples (n = 91) collected from headwaters to the open ocean, including samples subjected to laboratory treatments, with the original MLB_L survey (n = 37; D'Andrilli et al., 2015), totaling 128 samples. Based on our reassessment of the MLB approach using a more diverse data set of environmental and experimental samples, we suggest that the concept of lability thresholds may be usefully extended into the context of abiotic reactions, beyond the conventional applications to microbial metabolism alone.

2. Materials and methods

The molecular data set from D'Andrilli et al. (2015) was augmented and diversified by analyses of environmental samples from freshwaters, marine waters, soils, plants, and fossil organic hydrocarbons across the United States, mostly from the greater Mississippi River basin (Fig. 1, Table 1). We assessed the updated data set with three approaches. (1) We ranked each sample in terms of MLB_L percentages, according to the procedure in D'Andrilli et al. (2015). For this approach, 31 samples (Table 1) were analyzed and integrated into an augmented table summarizing both original and new information (Table S1) using the same organization scheme from the original study. (2) Patterns in MLB_L were compared more specifically across laboratory experiments on DOM and OM processing, such as heterotrophic microbial degradation, solar irradiation photochemical processing, and thermal decomposition by combustion and pyrolysis. We compared the changes in MLB_L across biotic and abiotic processes to identify trends in lability (66 samples). (3) Patterns in MLB_L were compared across human-induced environmental gradients in the field, such as eutrophic waterways with nitrogen (N) loading from fertilizers and agricultural management. We compared changes in MLB_L with anthropogenic influences and applied the trends identified in laboratory experiments to decipher potential processing mechanisms responsible for the observed signals (10 samples).

Ecosystem or experiment types considered in the three approaches to this synthesis were not represented in the original effort, expanding perspective on how lability indices may be expected to vary. The updated synthesis broadens the consideration of lability to riparian litter leachates, low-to-high order rivers, soils, forested streams, pyrogenic organic matter (biochar) leachates, and petroleum. Each approach builds progressively to define a broader perspective on lability based on more digestible summaries of FT-ICR MS data.

2.1. Description of samples

2.1.1. Expansion of the MLB_L data set from natural systems

Samples included to reevaluate the MLB approach and fill deficiencies with the original study were: Gulf of Mexico seawater (n = 1), fossilized hydrocarbons in the form of oils (n = 2), Minnesota forested streams (n = 4), Glacier National Park, Montana, Grinnell Glacier lakes (n = 4), Mississippi River International Humic Substances Society (IHSS) standard (n = 1), Sourdough Creek in Bozeman, Montana (n = 1), Yellowstone Lake in Yellowstone National Park, Wyoming (n = 1), Yellowstone River headwater in Yellowstone National Park, Wyoming (n = 1), tributary streams to the Gallatin and Missouri Rivers in Big Sky, Montana (n = 4), montane plant litter leachates (n = 3), semi-arid soils in Bozeman, Montana (n = 6), and southeastern USA plant biochar leachates (n = 3). A total of 31 samples from natural systems were added for reassessing the MLB approach, and the remainder of this section provides a detailed description of the added samples.

One sample representative of marine systems included a Gulf of Mexico seawater sampled by the Louisiana Universities Marine Consortium. Samples of fossilized carbon extracted from marine seabed drilling included a surrogate of Macondo oil representative of the Gulf of Mexico benthic oil supply (BP-operated Macondo Prospect - provided by BP August 2011, chain of custody number 20110803-Tarr-072) and heavy fuel oil (1621e from the National Institute of Standards and Technology; NIST).

Mountain headwater samples included tributaries of the Gallatin and Missouri Rivers (West Fork of the Gallatin River and Sourdough Creek, Montana, USA), montane lakes in Glacier and Yellowstone National Parks (Montana and Wyoming, USA), and the Yellowstone River headwaters (Wyoming, USA). The Yellowstone River headwaters were sampled in a remote area of a US National Forest, in contrast with Sourdough Creek that was sampled in Bozeman, Montana, where it runs adjacent to agricultural fields and residential areas. The Yellowstone River headwaters, the West Fork of the Gallatin River, and Sourdough Creek have snowmelt driven hydrologic regimes, receive a variety of plant litter, and are adjacent to vastly different land use. Samples from streams and lakes in Wyoming and Montana were collected in 1.0 L clean, combusted (4 h at 425 °C) glass bottles, filtered at 0.45 μm with glass fiber filters, and prepared for FT-ICR MS by solid phase extraction
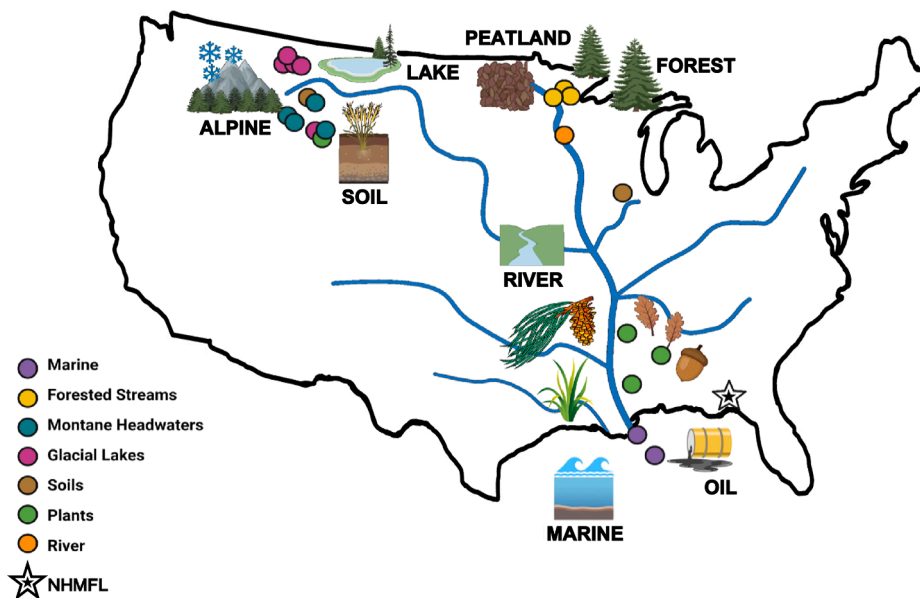
Fig. 1. Conceptual drawing of the greater Mississippi River Basin, USA, where our samples for organic matter characterization by FT-ICR MS analysis were collected. The location of the National High Magnetic Field Laboratory (NMHFL) is shown as a star (Tallahassee, Florida, USA).

(SPE; PPL cartridges, Agilent Technologies).

Stream samples representative of non-mountainous headwaters were obtained from forested streams at the Marcell Experimental Forest (Minnesota, USA). Forested streams at the Marcell Experimental Forest drain peatlands and ultimately flow to the Mississippi River (Fig. 1) (Sebestyen et al., 2021). The Marcell Experimental Forest peatlands were established as field sites for monitoring in the 1960s by the United States Department of Agriculture (USDA) Forest Service and represent an important hydrological research site in a low-topographic relief landscape that contrasts with other mountainous terrains (typically characteristic of river ecosystem headwaters) (Sebestyen et al., 2021). For this work, we focused on four Minnesota forested stream sites (S1, S2, S3, and S6) that represent diverse forested stream catchments of fens and bogs with a variety of vegetation types. Data from these streams are unique from the previously published peatland data from Minnesota (D'Andrilli et al., 2010; Tfaily et al., 2013; D'Andrilli et al., 2015) because these peatlands have no history of anthropogenic drainage. For detailed descriptions on the Marcell Experimental Forest catchment topography and characteristics for multiple sites, see Sebestyen et al. (2011); Sebestyen et al. (2021). The Minnesota forested stream samples were filtered with 0.7 µm glass fiber filters prior to SPE (PPL cartridges).

Natural organic matter (NOM) from a higher order river was previously sampled from the Mississippi River near Minneapolis. This sample was collected near the intake for the City of Minneapolis Water Works at the north edge of the city in Fridley (Minnesota, USA) for the purpose of providing a reference material from the IHSS (MissNOM #1R110N). For our study, MissNOM was obtained from the IHSS, dissolved in ultrapure water (Milli-Q), and subsequently extracted by SPE (PPL cartridge).

Samples representative of soil and plant derived OM included several cultivated semi-arid soils (Montana, USA) (Romero et al., 2018), montane litter leachates (D'Andrilli et al., 2019), and biochar leachates of southeastern US leaves, grasses, and pine needles (Podgorski et al., 2012; Wozniak et al., 2020). For further details on these samples see sections 2.1.2 and 2.1.3.

2.1.2. Controlled laboratory experimental samples for lability comparisons

Using data from a 44-day microbial degradation incubation experiment reported in D'Andrilli et al. (2019), we compared MLB_L values of three montane litter leachates (sources: riparian grass, leaf, and pine needle) mixed with local stream water (Sourdough Creek, Bozeman,

Montana, USA). Results from leachate incubations were interpreted as the effects of heterotrophic microbial transformations on DOM composition and character initially after mixing, at the peak of microbial growth (2nd day of incubation), and at 44 days (D'Andrilli et al., 2019). Nine samples are included from the incubations, i.e., individual mixtures of grass, leaf, and pine needle leachates with the Sourdough Creek stream water collected on days 0, 2, and 44. Plant litters were dried at 25 °C and manually ground into coarse particulates. Particulates were mixed with deionized water, agitated every 6 h for 24 h, and then filtered with combusted 0.45 µm glass fiber filters to collect 1 L of leachate solution. The leachates, stream water, and all incubated samples were filtered with 0.2 µm Sterivex™ filters and prepared for FT-ICR MS by SPE (200 mg PPL cartridges). SPE volumes were 100 mL for incubated samples. Incubations occurred in the dark at 29 °C until dissolved organic carbon concentration consumption was < 0.25% per day (D'Andrilli et al., 2019).

Samples of 'light' oil and 'heavy' fuel oil oxygenated DOM products after solar simulated light exposure on seawater (laboratory simulated photo-processing) were generated from a photodegradation experiment first reported in Zito et al. (2019). The oil samples were categorized as parent oils (light and heavy), however, the photo-processed oils (light and heavy with light exposure across 60 days) and dark controls were not previously reported. We use those data to track compositional changes in oil OM photo-processing over rapid (the first few hours and days) and extended timescales (~10–60 days) with the MLB approach. Light oil irradiated sample time points (n = 21) were collected at days 1.5, 3, 4.5, 6, 7.5, 9, 10.5, 13.5, 15, 18, 24, 27, 30, 36, 42, 48, 54, 58.5, and 60; including the two controls at days 1 and 60. Heavy fuel oil irradiated sample time points (n = 20) were the same as the light oil, except for day 36. The time points were selected based on irradiated hours 6, 12, 18, 24, 30, 36, 42, 54, 60, 72, 96, 108, 120, 144, 168, 192, 216, 234, and 240 and converted to approximate days for this work (King et al., 2014). Gulf of Mexico seawater (35 ppt salinity, pH 8.3, and dissolved organic carbon concentration of 0.125 mmol/L) was filtered using 0.27 µm (Advantec MFS GF75) glass fiber filters prior to mixing with the light and heavy fuel oils; therefore, changes in chemical composition were evaluated as abiotic dark and light only, without biological changes from microbial metabolism. Photochemically weathered oil was collected and dissolved in 1:1 toluene:methanol prior to FT-ICR MS (Zito et al., 2019). The seawater was irradiated for 12 h to

Table 1

Organic matter samples highlighted as the new data in this study integrated with the original samples in D'Andrilli et al., (2015). Approach numbers refer to samples used in the extended survey of the MLB approach (1), samples used in controlled incubations to track changes in lability with biotic and abiotic processes (2), and samples used for lability comparisons across anthropogenic influences (3). The values following commas in the Sample No. column indicate the number of samples used for incubations. OC; organic carbon.

Environment	Sample Name	Location	OC Concentration	Reference	Sample No.	Approach	Notes
Glacial	Pony Lake Fulvic Acid[+++]	Pony Lake, Antarctica	1.66 – 2.49 mM	This study	1		IHSS Reference sample
Marine Seawater	LUMCON Seawater	Gulf of Mexico, USA	125 µM	This study and Zito et al. 2019	1	1	Salinity 35 PSU and pH 8.3
Oil	Macondo Oil	Gulf of Mexico, USA	8.33 – 20.8 mM	This study and Zito et al. 2019	1, 21	1 & 2	BP, #20110803-Tarr-072, irradiated in seawater over 60 days
	Heavy Fuel Oil (benthic origin)	–	8.33 – 20.8 mM	This study and Zito et al. 2019	1, 20	1 & 2	NIST Standard Reference Material 1621e irradiated with seawater for 24 and 240 h
Terrestrial Freshwater	Forested Streams	Minnesota, USA	0.832 – 70.6 mM	This study and Sebestyen et al. 2021	4	1	Marcell Experimental Forest with streams emerging from bogs and fens
	Grinnell Glacier Lakes	Montana, USA	20.6 – 60.5 µM	This study	4	1	Glacier National Park collected in October 2014
	Mississippi River	Mississippi, USA	13.4 mM	This study	1	1	IHSS Natural Organic Matter #1R110N; MissNOM
	Sourdough Creek	Montana, USA	0.122 mM	D'Andrilli et al. 2019	1	1	Stream water
	Suwannee River Fulvic Acid II[+++]	Georgia, USA	1.66 – 2.49 mM	This study	1		IHSS Standard 2S101F
	Suwannee River [+++]	Georgia, USA	1.66 – 2.49 mM	This study	1		IHSS Natural Organic Matter
	West Fork of the Gallatin River	Montana, USA	83.3 – 192 µM	This study	4	1 & 3	Missouri River Headwaters: up and downstream of the golf course
	Yellowstone Lake	Wyoming, USA	0.145 mM	This study	1	1	Sample collected from the surface waters (6 m depth)
	Yellowstone River Headwaters	Wyoming, USA	85.8 µM	This study	1	1	Collected in September 2013 at Two Ocean's Pass
Soil	Arthur H. Post Agronomy Research Farm	Montana, USA	0.749 – 2.66 mM	This study and Romero et al. 2017, 2018	6	1 & 3	Fallow Wheat and Annual Cropping systems at 0–10, 10–20, and 20–30 cm
Plant	Brome Grass: Bromus sp.	Montana, USA	14.5 mM	D'Andrilli et al. 2019	1, 3	1 & 2	Grass leachate across a 44 day heterotrophic degradation incubation
	Douglas-Fir: Pseudotsuga menziesii	Montana, USA	21.7 mM	D'Andrilli et al. 2019	1, 3	1 & 2	Pine needle leachate across a 44 day heterotrophic degradation incubation
	Trembling Aspen: Populus tremuloides	Montana, USA	37.9 mM	D'Andrilli et al. 2019	1, 3	1 & 2	Leaf leachate across a 44 day heterotrophic degradation incubation
	Laurel Oak: Quercus laurifolia[+,+++]	Southeastern USA	0.683 – 2.58 mM	This study	1, 3	1 & 2	Biochar leachate: 3 h combusted at 250 °C or pyrolyzed at 400 °C and 650 °C
	Fakahatchee Grass: Tripsacum floridanum[++]	Southeastern USA	2.83 – 4.41 mM	This study	1, 3	1 & 2	Biochar leachate: 3 h combusted at 250 °C or pyrolyzed at 400 °C and 650 °C
	Loblolly Pine: Pinus taeda	Southeastern USA	2.83 – 4.41 mM	This study	1, 3	1 & 2	Biochar leachate: 3 h combusted at 250 °C or pyrolyzed at 400 °C and 650 °C

[+] Pioneering work on the FT-ICR MS instrument from the NHMFL using the DAPPI ionization technique on the solid biochars; Podgorski et al., 2012.

[++] First reports of ESI FT-ICR MS biochar leachate data from Old Dominion University (12 T FT-ICR MS instrument); Goranov et al., 2020 and Wozniak et al., 2020.

[+++] Data collected in 2020 (Fig. S1) following recommendations by Hawkes et al. (2020).

reduce background DOM composition and subsequently extracted using 50 mg SPE PPL cartridges to a final concentration of 50 mg C/mL.

Samples of solid phase and water extractable biochar undergoing thermal degradation were included in our synthesis. The samples originated from Laurel Oak (hereafter, Oak), Loblolly Pine (hereafter, Pine), and Fakahatchee Grass (hereafter, Grass), which grow abundantly in the southeastern US. Litter biochar and their leachates from these plants have been used extensively over the last 13 years to study thermal decomposition processes (e.g., combustion at 250 °C and pyrolysis at 400 °C and 650 °C) and their OM products (Zimmerman, 2010; Mukherjee et al., 2011; Podgorski et al., 2012; Bostick et al., 2018; Bostick et al., 2020; Goranov et al., 2020; Wozniak et al., 2020). Thermal decomposition (e.g., combustion and pyrolysis) breaks down OM similar to wildfires or controlled burns and represents another process cycling carbon in the environment. Recently, the water extractable portion after combustion and pyrolysis (i.e., dissolved black carbon filtered at 0.7 µm with glass fiber filters) that would likely be incorporated into soils, freshwaters, and marine waters were reported for Oak and Grass at two

pyrolysis temperatures (Goranov et al., 2020; Wozniak et al., 2020). In our work, we extended biochar OM characterization to include another source, Pine, and evaluated the data set using the MLB approach to provide a new perspective on compound degradation and formation as a function of combustion and pyrolysis. Temperatures used for thermal degradation included combustion at 250 °C and pyrolysis at 400 °C and 650 °C. We analyzed the results from each biochar exposed to the three thermal degradation temperatures (n = 9) and compared them with the original material. Water extractable DOM from the solid phase was generated (80 mL) and filtered sequentially through 1.0 µm (pre-combusted Fisherbrand G2) glass fiber filters and 0.45 µm (Millipore mixed cellulose ester) filters and prepared for FT-ICR MS by SPE (PPL cartridges) (Wozniak et al., 2020).

2.1.3. Samples for lability comparisons across anthropogenic influences

Analyses of samples from a stream influenced by humans are included from the West Fork sub-basin of the Gallatin River Watershed (Big Sky, Montana, USA), which has growing water quality issues related

to extensive increases in land use development in recent decades (Gardner and McGlynn, 2009; Gardner et al., 2011). Data added for this study include sites upstream and downstream of a stream-adjacent golf course that uses nitrate-rich treated wastewater for irrigation. These sites were chosen to test the effect of chronic N loading on DOM composition and stream ecosystem processes and were selected to be as similar as possible in an attempt to isolate the influence of N loading between the sites (Gardner and McGlynn, 2009; Gardner et al., 2011). One upstream and one downstream sample was collected in August 2015 and October 2016 (total samples n = 4) to highlight potential seasonal differences in the influence of algal growth typical in the late summer and early fall (Gardner and McGlynn, 2009). Samples were collected in 1.0 L combusted glass bottles, filtered at 0.45 μm using glass fiber filters, and prepared for FT-ICR MS by SPE (200 mg PPL cartridges).

Samples were also included from a study exploring changes in the molecular composition of soil DOM isolated from a semi-arid agro-ecosystem in southwestern Montana, USA (Romero et al., 2018). Samples were characterized across two winter wheat (*Triticum aestivum* L.) based cropping systems, conventional till fallow-wheat (FW), and no-till continuous cropping annual-wheat rotation (AW) sampled at three depth intervals (0–10, 10–20, and 20–30 cm; n = 6 samples). Conventional till with summer fallow has crop residue that is plowed into the soil after harvest, with fields left unsown (suppressed vegetation growth) for a growing season to accumulate soil water (Tanaka et al., 2010). No-till with continuous cropping has crop residue, including roots and any surface biomass not harvested, that is left in place between plantings for consecutive growing seasons (i.e., without a fallow season). Conventional till FW was selected to represent profiles with apparent soil organic carbon (C) losses, mainly due to plowing and more rapid plant-C turnover, whereas AW depicted profiles with apparent soil organic C gains and less rapid plant-C turnover in surface and subsurface layers (Engel et al., 2017). Water extractable DOM from the solid phase was generated using 18 mL of deionized water and 2 mL of 1 mol/L $CaCl_2$ shaken, allowed to settle, and then filtered (15 mL of supernatant through a 0.45 μm nylon filter) prior to SPE (200 mg PPL cartridges) for FT-ICR MS (Romero et al., 2018).

2.2. Sample preparation

DOM extracts (2 mL) from their respective PPL cartridges were eluted with HPLC grade methanol and stored in clean, combusted amber glassware at or below 4 °C in the dark prior to FT-ICR MS analysis. Sample collection volumes varied depending on availability, dissolved organic C concentration, and PPL SPE cartridge loading instructions (Dittmar et al., 2008). These sample preparation methods are commonly applied in the organic geosciences to analyze molecular formulas and chemical characterizations of DOM by FT-ICR MS and to infer C cycle processes within and across ecosystems.

2.3. Electrospray ionization and FT-ICR MS analysis

All samples were externally ionized using Electrospray Ionization (ESI) in negative ion mode, which produced singly charged, gaseous negative ions. Ions were produced by a custom-built micro-electrospray ionization source (Emmett et al., 1998). The experimental parameters for ESI were: 50 μm i.d. fused-silica tube, syringe pump flow rate 0.5–1.0 μL/min, needle voltage –2200 to –2700 V, tube lens –300 to –350 V, and heated metal capillary operated at 7.21–10.5 W. These settings were determined from previous negative ion mode ESI FT-ICR MS experiments prior to 2011 and then reevaluated over time to produce reliable and reproducible data (Purcell et al., 2007; D'Andrilli et al., 2010; D'Andrilli et al., 2013; Hawkes et al., 2020).

The new data were obtained between 2011 and 2021 with the custom-built 9.4 T superconducting magnet FT-ICR mass spectrometer at the NHMFL in Tallahassee, Florida, USA (Blakney et al., 2011; Kaiser

et al., 2011). Excitation ranged from m/z 200–1500 at frequency sweep 50 Hz/μs, and octopole ion guide frequencies were maintained at 2.0 MHz. FT-ICR MS parameter ranges incorporate ten years of 9.4 T FT-ICR MS acquisition at the NHMFL and were selected based on previously characterized DOM samples and optimized for each study, as outlined in D'Andrilli et al. (2015). Mass spectra were generated with co-added multiple (10–200) time domain acquisitions that were Hanning apodized and zero-filled once before fast Fourier transformation and magnitude calculation (Marshall and Verdun, 1990).

2.4. DOM calibration and chemical assessments

FT-ICR MS data were internally calibrated for DOM molecular formula assignments with highly abundant methylene homologous $-CH_2$ series commonly found in NOM mixtures, with mass to charge ratios ranging from 200 to 900 (Sleighter and Hatcher, 2008; Savory et al., 2011). Calibration produced assigned elemental compositions with root mean square mass measurement error < 1 ppm for singly charged negative ion analyte species. NHMFL software generated calibrated peak lists for molecular formula assignment, limited to peaks of magnitude greater than 6 times the baseline root mean square noise – a conservative threshold that allows for reliable comparison of DOM and OM from different sources. DOM analyte ions for this study were singly charged, confirmed by the naturally occurring ^{13}C-isotopic mass spectral peak separation pattern (1.0034 Da) between ions differing in elemental composition by $^{12}C_c$ vs. $^{12}C_{c-1}^{13}C_1$ (Limbach et al., 1991; Brown and Rice, 2000; Kujawinski et al., 2002).

Molecular formula assignment using 9.4 T negative ion mode ESI FT-ICR MS data has been previously described in detail (Stenson et al., 2003; D'Andrilli et al., 2013; D'Andrilli et al., 2015). Elemental compositional constraints were modeled after those reported for NOM characterization by the same 9.4 T FT-ICR MS instrument and elemental compositions containing $C_cH_hN_nO_oS_s$ were considered for this work (Stenson et al., 2003; D'Andrilli et al., 2013; D'Andrilli et al., 2015). Also, hydrocarbon molecular assignments without O were only considered for the oil samples (oil organic composition molecular backbone = C_cH_h versus DOM = $C_cH_hO_o$). We classified elemental combinations of N and/or S in $C_cH_hO_o$ containing DOM to define its heterogeneity (i.e., $C_cH_hO_oN_{0-3}S_0$, $C_cH_hO_oN_{1-2}S_1$, and $C_cH_hO_oN_0S_1$). Molecular compositions for DOM from the Glacier and Yellowstone National Park lakes, mountain headwater streams, Yellowstone Lake, the Minnesota forested streams, and oils were assigned by PetroOrg software (Corilo, 2014) and the montane litter leachates were assigned by EnviroOrg (NHMFL software by Yuri Corilo © EnviroOrg™, Florida State University: 2016). Molecular formula assignments included all possible naturally occurring molecular combinations of C, H, N, O, and S within these DOM ranges: $^{12}C_{1-100}$, $^1H_{1-200}$, $^{14}N_{0-3}$, $^{16}O_{2-50}$, and $^{34}S_{0-1}$. Oils followed the same range except with $^{16}O_{0-50}$. Biochar DOM molecular formulas were assigned manually and confirmed using NHMFL software following three criteria. Assignments were: (1) specific to ion peaks for homologous series above the S/N threshold; (2) had mass error < 1 ppm; and (3) had ^{13}C peak confirmation and specified mass spacing patterns (Podgorski et al., 2012). Formula confirmation of PetroOrg assignments using NHMFL software were based on mass spectral spacing patterns and the same criteria as has been previously used for manual composition assignments (D'Andrilli et al., 2015). Without confirmations of fundamental mass spectral spacing patterns of highly resolved peaks, assigning individual peaks to DOM molecular formula would not be possible within a reasonable error margin (e.g., < 1 ppm) (Stenson et al., 2003; D'Andrilli et al., 2013). Further discussions on the utility of monoisotopic mass spectral patterns for DOM characterization by FT-ICR MS were previously published (Stenson et al., 2003; D'Andrilli et al., 2015; D'Andrilli et al., 2020; Cooper et al., 2022).

DOM composition analysis began with the formula information itself using molecular masses and elemental compositions (e.g., mass ranges, number of molecular formulas, which elements, and how many of each).

Then, analyses extended to chemical characterization and interpretation such as compartmentalizing data on van Krevelen diagrams based on relative hydrogen and oxygen content with respect to C (H/C and O/C ratios). Detailed assessment of composition was based on the numbers of C, H, N, O, and S atoms per assigned formula and subsequently used to calculate double bond equivalence, hydrogen saturation (hydrogen-to-carbon ratio; H/C), oxygenation (oxygen-to-carbon ratio; O/C) (Kim et al., 2003), aromaticity (Koch and Dittmar, 2006), and degree of heterogeneity (composition percentages of N and/or S) (D'Andrilli et al., 2013). The proportions of DOM biolability per sample, denoted by the MLB_L metric, were calculated using the MLB following established methods (D'Andrilli et al., 2015). Briefly, MLB_L percentages are calculated as 100% times the fraction of total molecular formulas over the range of O/C from 0 to 1.2 having H/C greater than or equal to the MLB threshold of 1.5; Equation (1) (D'Andrilli et al., 2015).

$$\% \, MLB_L \,=\, 100 \times \left(\frac{(\# \,\, of \,\, molecular \,\, formulas \,\, with \,\, H/C \,\geq\, 1.5)}{(total \,\, \# \,\, of \,\, molecular \,\, formulas)} \right) \quad (1)$$

For MLB_L percentages among heterogeneous molecules (i.e., atomic constituents with N- and/or S-containing atoms), we followed the same MLB_L calculation using the number of formulas in each heterogeneous group as the respective totals; example in Equation (2) (D'Andrilli et al., 2015).

$$\%MLB_L \, C_cH_hO_oS_1 = 100 \times \left(\frac{(\# \,\, of \,\, C_cH_hO_oS_1 \,\, molecular \,\, formulas \,\, with \,\, H/C \,\geq\, 1.5)}{(total \,\, \# \,\, of \,\, C_cH_hO_oS_1 \,\, molecular \,\, formulas)} \right) \quad (2)$$

Equation (2) shows an example for calculating the % MLB_L for the S-containing DOM heterogeneous group $C_cH_hO_oS_1$ and can be used for remaining heterogeneous groups ($C_cH_hO_oN_1$, $C_cH_hO_oN_2$, $C_cH_hO_oN_3$, $C_cH_hO_oN_1S_1$, and $C_cH_hO_oN_2S_1$) by substituting the group of choice for $C_cH_hO_oS_1$ in Equation (2). Percent MLB_L can also be calculated for additive heterogeneous contributions, such as total N without S ($C_cH_hO_oN_{1-3}$) using Equation (3).

$$\%MLB_L \, C_cH_hO_oN_{1-3} = 100 \times \left(\frac{(\# \,\, of \,\, C_cH_hO_oN_{1-3} \,\, molecular \,\, formulas \,\, with \,\, H/C \,\geq\, 1.5)}{(total \,\, \# \,\, of \,\, C_cH_hO_oN_{1-3} \,\, molecular \,\, formulas)} \right) \quad (3)$$

Recalcitrant DOM percentages (MLB_R derived from the fraction with H/C < 1.5) were calculated as the complement of MLB_L (i.e., 100% - MLB_L) both across the full range of O/C and within each heterogeneous group (D'Andrilli et al., 2015). The MLB_L percentages were compiled for all samples to allow comparisons across environments and sample types (Table S1) and to allow comparisons with the original results reported in D'Andrilli et al. (2015).

3. Results and discussion

The data in this study provided a larger distribution of MLB_L data for comparison, filling in perceived gaps in the previous study from different environments (Fig. 2). Patterns in DOM and OM biolability across diverse systems demonstrate oils, soils, litter leachates, and biochar leachates are comprised of more hydrogen saturated chemical

species than inland freshwaters of the previous study. Comparisons of the processing of OM and DOM from laboratory experiments reflect changes in MLB_L with both biotic and abiotic processes. Exploration of patterns of DOM biolability in human-influenced environments show smaller changes in MLB_L than in laboratory experiments. We found that evaluating MLB_L changes with laboratory experiments helped to interpret data comparisons in human-influenced environments. Variation in MLB_L percentages across the updated data set reflected OM and DOM with biolability from 0 to 49.1 % (Table S1). The new samples generally reflected a higher MLB_L than the previous study (Fig. 2a-c). Dominant patterns in biolability emerged with respect to variation in DOM and OM composition and character, suggesting the relevant processes affecting changes in composition (whether in the laboratory or field) and the environmental drivers of such changes. Values for MLB_L among the new samples ranged from 3.54 % to 49.1 %. Light oil after 60 days of irradiation had the most hydrogen saturated compounds (maximum % MLB_L) and Oak biochar leachate after thermal degradation had the least (minimum %MLB_L; Table S1 and Fig. 2b). Light oil demonstrated similar MLB_L as marine and isolated glacial environments dominated by microbes from the original survey (Fig. 2a–b, Table S1). The MLB_L for the irradiated light oil sample was 2.6 % greater than the Cotton Glacier Stream (an Antarctic supraglacial stream; Table S1) (D'Andrilli et al., 2015). To date, higher MLB_L values have typically been associated with marine DOM, glacial OM, and/or non-oxygenated OM chemical species from primary producers and energy rich materials favored in microbial metabolism (Chipman et al., 2010; D'Andrilli et al., 2017; Smith et al., 2018; King et al., 2019). With the addition of the OM composition in oil after irradiation, we demonstrate the potential for higher MLB_L values to reflect photo-processing. Across the combined data distributions (Fig. 2c), the mean MLB_L was 13.4 % and the median was 11.1 % indicating the dominance of DOM and OM with low hydrogen saturation across diverse ecosystems. Ecosystem types were generally grouped by biolabile compositional character as summarized by decreasing MLB_L in the following order: oil, glacial, marine, litter leachates, biochars, soils, inland freshwaters, and peatland porewaters (Fig. 2a–b; Table S1). Like the original survey, higher DOM MLB_L percentages represent a larger number of organic compounds produced by microorganisms and favorable to microbial degradation and/or turnover in ecosystems characteristically dominated by microbial processes and with relatively minimal or no higher-plant inputs (e.g., Antarctic, high-alpine and high latitude glacial, and marine). Lower DOM MLB_L percentages represent ecosystems with dominant DOM contributions from allochthonous sources and/or the accumulation and storage of C, as seen in peatlands.

3.1. Comparisons of freshwater DOM MLB_L, heterogeneity, and ecosystem influences

Ranges in MLB_L from the new data for stream, lake, and river DOM were 3.68 – 16.8 % (Table S1) with a Minnesota forested stream (S3) as

the lower boundary and Glacier National Park's Grinnell Glacier pro-glacial lake as the upper boundary. Grinnell Glacier's proglacial lake is a relatively young feature of the Grinnell watershed compared to the age of the glacier, forming from a major calving event ~ 1946 (Dyson, 1948). It is the only lake in the Grinnell watershed above the tree line and is less influenced by adjacent soil development relative to its downstream lakes and the other high elevation lake in the study from Yellowstone National Park (Figs. S2-3, Tables S2-3). Grinnell Glacier lake DOM MLB$_L$ values decreased with distance downstream of the glacier, i.e., the proglacial lake, Grinnell Lake, Lake Josephine, and Swiftcurrent Lake. In terms of limnetic types and geographic influences, lake DOM had the highest MLB$_L$, followed generally by mountainous headwater streams, bog-influenced forested headwater streams, a high-order river, and a fen-influenced forested headwater steam (Tables S1-3).

The Yellowstone River headwaters (1st order) and Sourdough Creek (3rd order stream) DOM had similar MLB$_L$ (6.49 % and 6.82 %) yet differ by heterogeneous composition (Fig. S3, Table S3). We speculate that nutrient loading from anthropogenic activity is likely responsible for greater heterogeneous composition of DOM in Sourdough Creek compared to the Yellowstone River headwaters, because Sourdough Creek was sampled in a location likely strongly influenced by agricultural and residential development in the Gallatin Valley. Therefore, a lack of DOM heterogeneity may be an indicator of nutrient limitations providing another way to think about FT-ICR MS data and land use more broadly.

The Yellowstone River headwater and Sourdough Creek MLB$_L$ values were lower than the glacially fed lakes (including Yellowstone Lake) and the Minnesota forested stream site S6, but greater than forested stream sites S1, S2, and S3 and the Mississippi River NOM isolate (Table S1). In northern Minnesota, various peatland types (e.g., bog, fen) cover vast areas with waterlogged, C-rich soils (Heinselman, 1963; Wright, 1972; Glaser et al., 1981), which likely affect the DOM composition. The four Minnesota forested stream sites ranged in MLB$_L$ from 4.33 % to 6.98 %. The S6 stream (MLB$_L$ = 6.98 %; Tables S1 and S4) drains uplands and a bog, both with conifer cover (Sebestyen et al., 2021). The S6 stream shared similar chemical character with DOM from the deep bog waters of the Minnesota Lost River peatland (D'Andrilli et al., 2015), Yellowstone River headwaters, and Sourdough Creek (Fig. S3). Minnesota forested stream sites S1 (MLB$_L$ = 5.36 %) and S2 (MLB$_L$ = 4.50 %) receive inputs from uplands with deciduous cover and with coniferous cover on the bogs (Sebestyen et al., 2021). Both S1 and S2 shared similar DOM chemical character and composition except for the $C_cH_hO_oN_2$

chemical species in S2 (Fig. S4, Table S4). The peatland near S3 (MLB$_L$ = 4.33 %), with more S-containing species than S1 and S2, is a tamarack-shrub fen, receiving groundwater input from the surrounding aquifer and peat (Bay, 1967; Sebestyen et al., 2021). DOM character from S1 and S3 were similar to other northern Minnesota bog and fen porewaters (Tfaily et al., 2013; D'Andrilli et al., 2015). Low MLB$_L$ values were expected for Minnesota forested stream DOM due to peatland influences dominated by recalcitrant OM that reflects C accumulation that exceeds C degradation by microbes.

MLB$_L$ from the Mississippi River IHSS reference (MissNOM) isolate (4.51 %) was only just higher than that of Minnesota forested stream site S3. Anthropogenic impacts (e.g., effluents from wastewater treatment plants) are likely a large influence on the river composition and character (Chin et al., 2023) and may be responsible for increased heterogeneous DOM, but further sampling efforts and comparisons with the IHSS sample and field samples would be needed to identify anthropogenic imprints on Mississippi River DOM beyond nutrient loading. Though the IHSS NOM isolate is highly processed compared to a field sample, it provides a single example (in this data set) of a high-order river with human and water treatment system inputs (Chin et al., 2023). The MissNOM isolate contained considerably more $C_cH_hO_oS_1$ chemical species (15.5 %) than Minnesota forested stream headwaters (S1, S2, S3, and S6: 0 – 7.37 %; Figs. S3-4, Tables S3-4). In fact, the $C_cH_hO_oS_1$ group was the most biolabile heterogeneous group overall with an average O/C of 0.62, a result consistent with Sourdough Creek and other higher-order rivers in the United States influenced by anthropogenic activity (D'Andrilli et al., 2015). Highly oxygenated DOM was a unique trend observed for the Minnesota samples across all chemical species, which may be an indicator of individual processing mechanisms (e.g., microbial and photo-processing). Therefore, evaluating trends in oxygenation coupled with the MLB$_L$ approach may provide another method to understand freshwater DOM in further detail.

3.2. Changes in DOM MLB$_L$ from carbon transformations isolated in laboratory experiments

3.2.1. Heterotrophic microbial degradation

The MLB$_L$ values increased from day 0 to day 2, and then decreased considerably by day 44 across all montane litter leachate OM sources (riparian grass, leaf, and pine needle; Fig. 3a). As heterotrophic degradation progressed, more oxygenated DOM was produced (Fig. 3b, Fig. S5). MLB$_L$ decreases were expected with heterotrophic degradation corresponding to the utilization of aliphatic DOM with protein-, amino
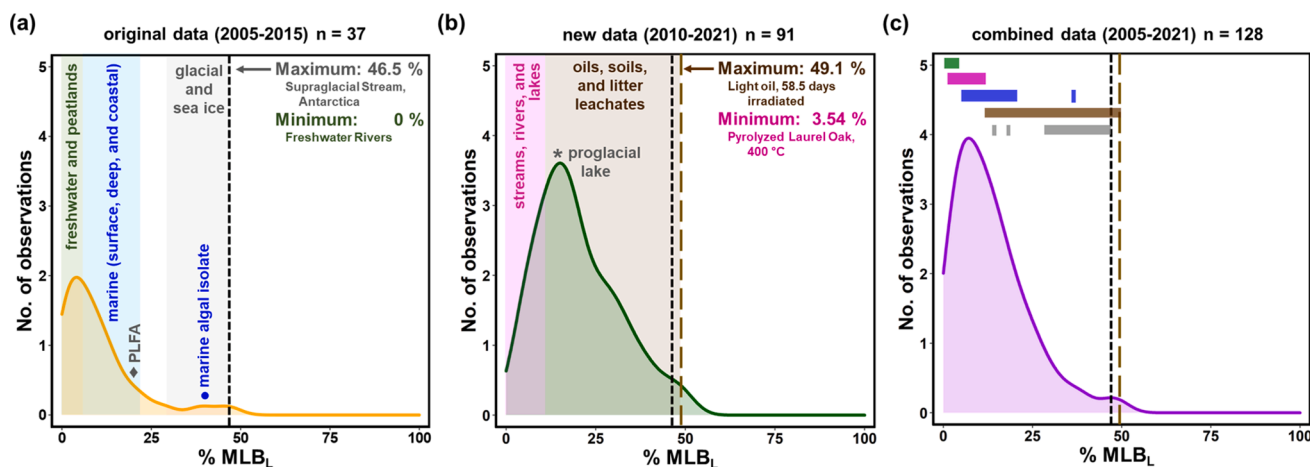

Fig. 2. MLB$_L$ frequency distributions across samples from a) the original lability study (D'Andrilli et al., 2015), b) the new samples in this study, and c) the combined distribution of both studies. The black and brown dashed lines show the maximum calculated biolability values and the colored bars in (c) show the general grouping of sample types and their overlap; colors consistent with font color in the shaded regions in (a) and (b). Distributions represent smoothed kernel density estimates of environmental samples. The MLB$_L$ values are available in Table S1. PLFA: Pony Lake Fulvic Acid.
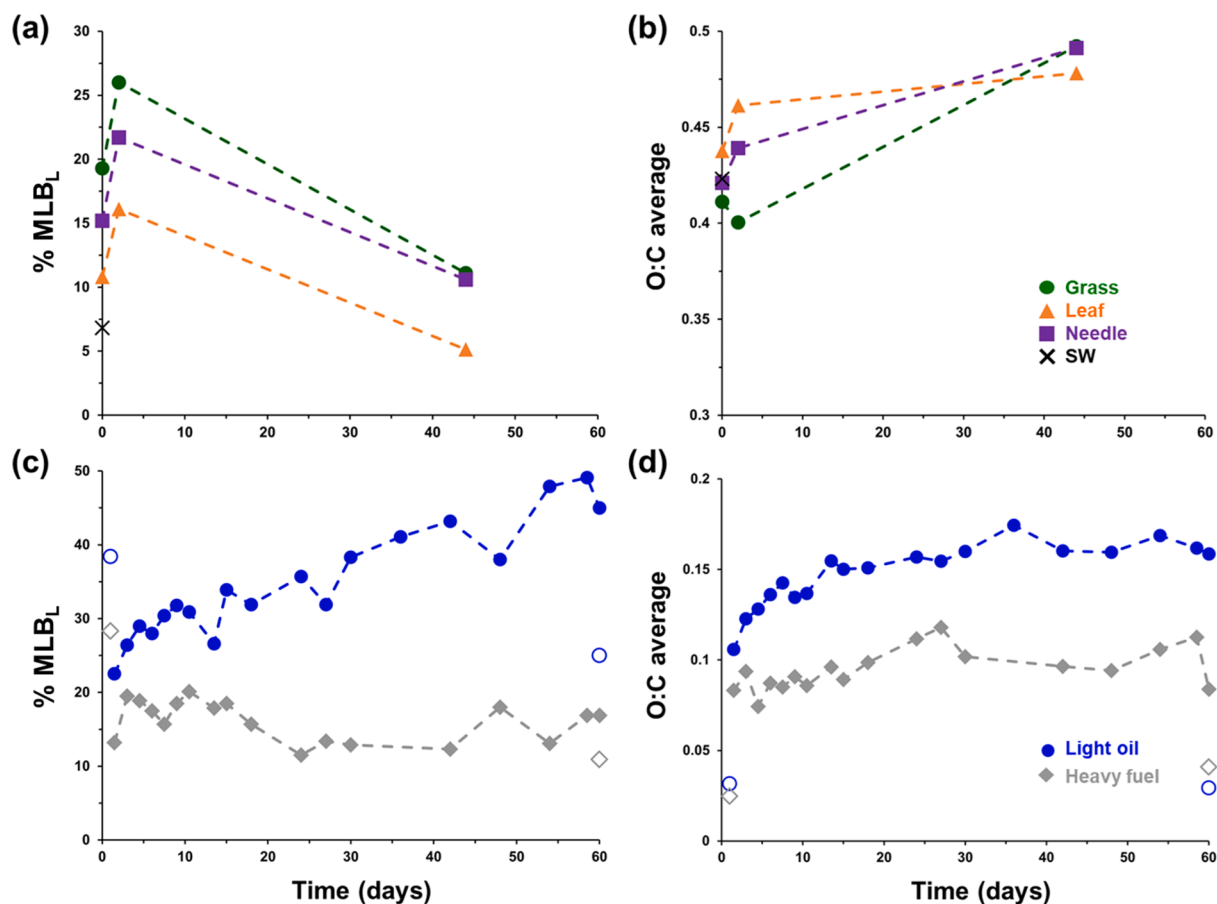
Fig. 3. Molecular composition metrics of MLB$_L$ percentages and oxygen-to-carbon ratio averages for (a–b) montane plant litter leachate dissolved organic matter (DOM) across a 44-day heterotrophic microbial degradation incubation (sources: grass, leaf, and needle) (D'Andrilli et al., 2019) and (c–d) two types of oil (light and heavy fuel) across a 60-day photodegradation experiment; open symbols denote dark controls. SW: Stream water from Sourdough Creek (Fig. S3c).

sugar-, and carbohydrate-like chemical character (D'Andrilli et al., 2019). Biodegradation created more complex, oxygenated lignin-like DOM composition with low hydrogen saturation by the end of the experiment (44 days). These results were consistent with trends observed for an algal-DOM sourced heterotrophic degradation experiment in river water without sunlight exposure, e.g., average MLB$_L$ and O/C before and after heterotrophic degradation were 38.8 % and 21.8 % and 0.39 and 0.48, respectfully (Chipman et al., 2010; D'Andrilli et al., 2015).

Comparisons of the FT-ICR MS data across the incubation revealed time-specific patterns of DOM transformations including biomass building, newly produced intermediates, C consumption, and production and accumulation of end products. Above the MLB, chemical changes specific to consumption were observed for highly oxygenated $C_cH_hO_o$ and $C_cH_hO_oS_1$ composition, whereas we speculate that the $C_cH_hO_oN_{1-2}$ changes were initially related to biomass growth and not longer-term metabolism. Newly produced biolabile DOM had distinct character for species containing $C_cH_hO_oN_2S_1$ at high O/C ratios that also served as reactive intermediates consumed by day 44 (Figs. S5-6). End products were dominated by lignin-like and/or carboxylic rich alicyclic molecules, known as CRAM (Hertkorn et al., 2006) at low hydrogen saturation, resembling DOM molecular composition often found in freshwater rivers (Figs. S1 and S3). Following the data across days 0, 2, and 44 makes heterotrophic degradation data on van Krevelen diagrams appear at specific H/C and O/C ratios with DOM chemical composition and character shifts linked to different microbial processes (Figs. S5-6). Analyzing these shifts together with the MLB$_L$ may provide a mechanism to help evaluate FT-ICR MS data from field samples that capture a multitude of ongoing processes.

3.2.2. Photochemical degradation

Oils undergoing photochemical degradation had differing changes in biolability depending on the original composition. The MLB$_L$ percentages of the oil data spanned a large range (10.9 – 49.1 %) describing substantial variation in the composition of hydrogen saturated oil after irradiation as well the highest MLB$_L$ value in the new dataset (49.1 %; Fig. 3c, Tables S1 and S5). Compared to the dark control, heavy fuel oil decreased in MLB$_L$ (28.3 – 13.2 %) after light exposure (Fig. 3c, Tables S1 and S5) due to oxygenation of the smaller hydrocarbons with photo-transformation into water-soluble oil products (Zito et al., 2019). The same was true for the light oil after irradiation (38.4 – 22.5 %) and a coastal river DOM sample from the original MLB$_L$ survey (Black River, North Carolina) (Gonsior et al., 2009; D'Andrilli et al., 2015). However, heavy fuel and light oil displayed different MLB$_L$ trends when exposed to light over short (6 days) and long (60 days) temporal scales (Fig. 3c), which we attribute to the original composition of the parent material (Fig. S7). Increasing trends in MLB$_L$ and oxygenation were more pronounced for the light oil (Fig. 3c-d). Overall, MLB$_L$ increased by 74.3 % and 43.1 % for light and heavy fuel oil with photodegradation. Comparing the two oils, the heavy fuel oil MLB$_L$ values were 73.4 % lower on average than the light oil. Again, these differences are attributed to the starting composition of the parent oil (Zito et al., 2019). The heavy fuel oil was enriched in aromatic and reduced hydrocarbons (Lemkau et al., 2010) compared to light oil (Fig. S7), and had fewer low molecular weight compounds commonly known to be rapidly oxygenated by photo-processing. Therefore, the heavy fuel oil took longer to degrade on the surface of seawater when exposed to sunlight. After extended photo-processing, the oil OM composition shifted to more saturated, highly oxygenated compound classes (Figs. 3c-d, S7)
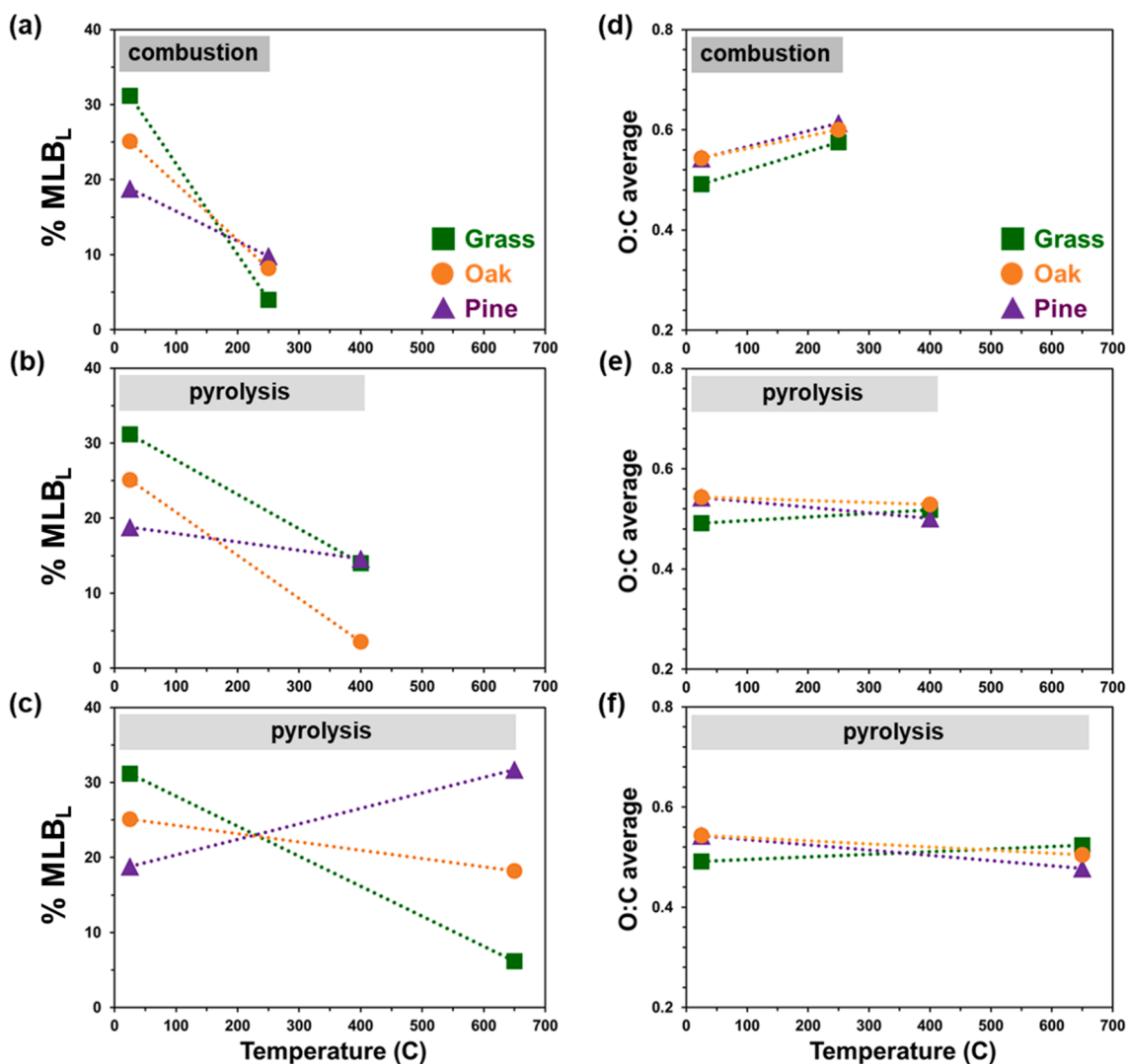
Fig. 4. Percent MLB$_L$ (a-c) and oxygen-to-carbon ratio averages (d-f) as a function of temperature for combustion (250 °C) and pyrolysis (400 °C and 650 °C) from FT-ICR MS data of Fakahatchee Grass (Grass), Laurel Oak (Oak), Loblolly Pine (Pine) biochar leachates. The parent biomass sources are depicted at room temperature (25 °C).

associated with continual processing of oil films lingering on seawater. More oxygenated photoproducts were produced across $C_cH_hO_o$, $C_cH_hO_oS_1$, and $C_cH_hO_oN_{1-2}$ chemical species by photo-processing (Fig. 3d) and specific forms of oxygenated products may depend on the source OM. Additionally, increases in heterogeneous content (N and/or S) may also result from the negative mode ESI selectivity bias of the seawater background (Fig. S8) over the oil analytes and ionizable carboxyl groups after photo-processing. Our results highlight compositional trends in OM reactivity that advance our understanding of "photolability" which creates opportunities to think more broadly about ecosystem processes, patterns, and products when interpreting van Krevelen diagrams from FT-ICR MS data.

3.2.3. Thermal decomposition

Combustion and pyrolysis generally caused decreases in biolability of leachates from Grass, Oak, and Pine biochars. Before thermal treatment, the leachate MLB$_L$ values were 31.2, 25.1, and 18.8 % for Grass, Oak, and Pine biochars, respectively. All thermally degraded DOM biochar leachates showed decreases in hydrogen saturated composition with each treatment temperature except Pine pyrolyzed at 650 °C (Figs. 4, S9, and Table S6). In fact, of all OM sources, Pine DOM biochar leachate had the least amount of MLB$_L$ changes with treatment

temperature. Pyrolysis at 400 °C created a shift in chemical character from the parent biomass with $C_cH_hO_o$ and $C_cH_hO_oN_{1-3}$ groups, a decrease in hydrogen saturation, an increase in oxygenation, and the formation of a distinct group of $C_cH_hO_oS_1$ at higher hydrogen saturation. These $C_cH_hO_oS_1$ species are likely individual or combined decomposition products from large molecules such as aromatics and CRAM (Hertkorn et al., 2006). Pyrolysis at 400 °C caused a decrease in MLB$_L$ for the leachates from Grass, Oak, and Pine biochars, reflecting the degradation of more hydrogen saturated chemical species and either the selective persistence or formation of recalcitrant and condensed aromatic moieties. The same trends were observed when pyrolysis temperature was increased to 650 °C for Grass and Oak biochars. The MLB$_L$ of thermally degraded DOM leachates (treated at 250, 400, and 650 °C) decreased by 27.2, 17.2, and 25.0 % for Grass, by 16.9, 21.4, and 6.9 % for Oak, and by 9.01 and 4.02 % and increased by 12.9 % for Pine, respectively. Increases in molecular oxygenation were observed for combustion at low heat treatment temperatures (250 °C), across all thermally degraded DOM leachates. But with pyrolysis at higher heating temperatures (400 and 650 °C), oxygenation decreased as DOM thermally decomposed for Oak and Pine leachates. Thermal decomposition products for pyrolyzed Grass DOM biochar leachate increased in oxygenation.

Pyrogenic OM and DOM are notably rich in condensed aromatic C, but highly variable in the degree of condensation, O-containing functional groups, molecular weight, and solubility in aquatic ecosystems (Masiello, 2004; Schneider et al., 2010; Podgorski et al., 2012; Wagner et al., 2018; Wozniak et al., 2020). The hydrophilic (dissolvable) fraction is likely the most environmentally mobile and reactive fraction (Wozniak et al., 2020) and thus represents the compounds most likely to undergo biogeochemical changes after wildfires. Evaluating the thermal decomposition products with temperature provides insight into the DOM molecular bonds and composition that control the timing of various DOM products during and following fires. For example, as wildfire temperatures fluctuate, the N- and S-containing DOM compositional changes must be dependent on a DOM binding site to be ionized and detected by FT-ICR MS. Without a $C_cH_hO_o$ binding site, N- and S-heterogeneous groups would be lost (i.e., outside of our analytical window). However, we observed heterogeneous composition with different chemical character across all temperatures and shifts in $C_cH_hO_o$ composition and character (Figs. S9 and S10). Therefore, heterogeneous molecular changes at various temperatures depend on the amount, chemical composition, and character of the $C_cH_hO_o$ species of the parent biomass *and* during decomposition.

Our analysis provides evidence that thermal decomposition temperatures and parent biomass materials may be targeted to achieve desired products needed to stimulate biogeochemical processes. For example, creating biolabile DOM enriched in S requires combustion of Grass, Oak, and Pine at 250 °C whereas N enrichment could be achieved with pyrolysis at 400 °C. These thermal decomposition procedures may be valuable avenues to stimulate ecosystem processes and/or maintain ecosystem stability such as building soil C stocks in coastal ecosystems and using decomposition products as an alternative to fertilizers for agricultural enrichment.

3.3. Trends in DOM MLB_L and ecosystem processes with anthropogenic forcing

3.3.1. Stream DOM MLB_L with chronic N loading from amenity development

Our study sites on the West Fork of the Gallatin River (a mountain headwater stream tributary of the Gallatin and Missouri Rivers) ranged in MLB_L from 4.99 to 8.76 % for samples collected during baseflow summer (2015) and autumn (2016) seasons in sequential years. Overall, the DOM showed little difference (0.06 %) in composition and MLB_L between upstream and downstream during summer 2015 (Figs. 5 and S11; Tables S1 and S7). Larger differences in chemical character, heterogeneity, and MLB_L were observed during autumn 2016, suggesting the accumulation or production of N_2-containing and more oxygenated DOM composition downstream (Fig. S11 and Table S7). Downstream MLB_L values each year were greater than upstream, though differences were < 1 %, which does not allow for meaningful differentiation in C quality by the MLB approach alone. The MLB_L was greater in autumn compared to summer (average MLB_L in autumn = 8.49 % and summer = 4.86 %), which could reflect interannual variation as well as the potential role of algae and algal senescence at the end of the growing season.

We used the relative abundances of % $C_cH_hO_o$ composition below the MLB to infer allochthonous DOM contributions from alpine soils which seemed to dominate the character relative to the potential influence of nutrient rich OM leaking from algal growth in the study sites. Perhaps assessment of the influence of autochthonous production needs to consider specific types of compounds (e.g., Table S7) or the variation in compounds released during growth stages of algal productivity (e.g., August versus October) to be detectable above the dominant character created by terrestrial and soil OM inputs. Therefore, we used the combination of percentages of compounds containing N, their chemical character (i.e., protein-like), and heterogeneous MLB_L values to infer increases in autochthonous DOM production, microbial biomass growth, and microbially produced biolabile DOM intermediates. For summer
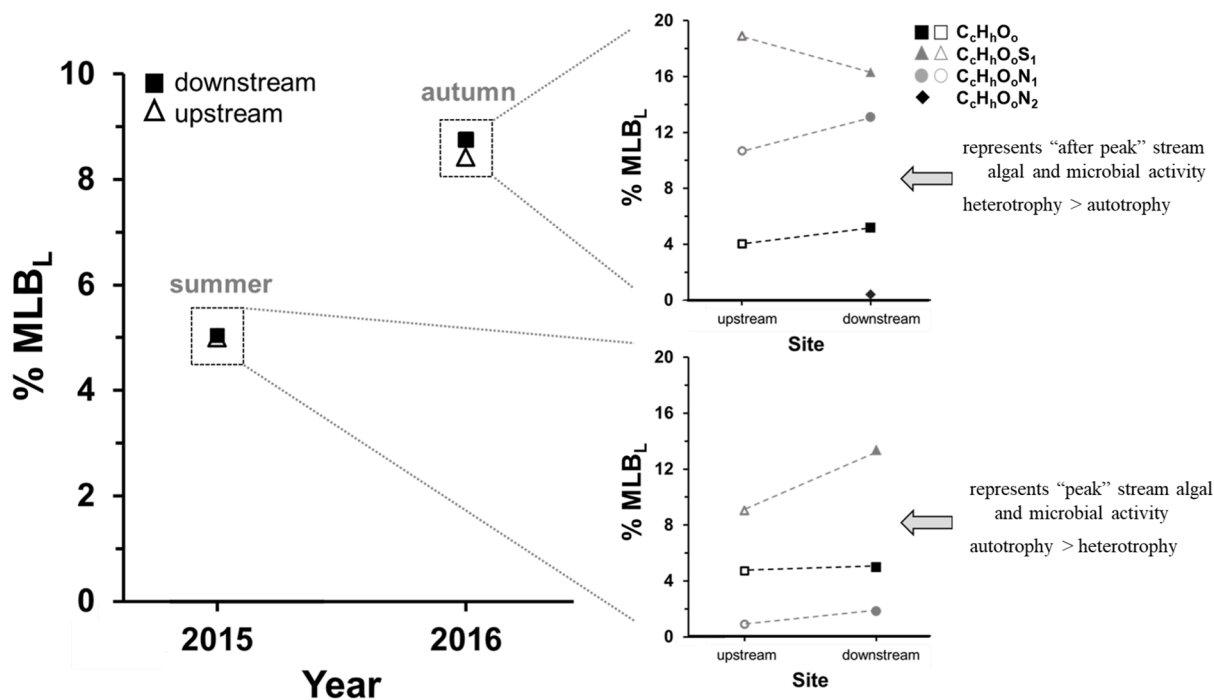

Fig. 5. Dissolved organic matter (DOM) molecular composition metrics of overall MLB_L and heterogeneous MLB_L for the stream samples collected from the West fork of the Gallatin River (Big Sky, Montana, USA) for summer 2015 and autumn 2016. The terms 'upstream' and 'downstream' refer to sampling locations on the river relative to the golf course adjacent to the reach between them. Heterogeneous MLB_L insets on the right represent "peak" and "after peak" microbial activity in the stream in different seasons. Black and white figure.

2015, upstream and downstream DOM composition was dominated by allochthonous inputs likely originating from watershed soils, characterized by the DOM composition centered within the lignin-like chemical class (H/C = 1 and O/C = 0.5; Fig. S11), common for stream flow contributions from vegetated soils (Figs. S2-S5). The differences in molecular composition between the upstream and downstream DOM were evident in increased heterogeneous nature, MLB_L, and protein-like contributions for the downstream site (Fig. S11 and Table S7). We suggest these differences arise from increased local algal production during the summer growing season (Fig. 5) (Schade et al., 2010). Additionally, the lack of N-containing protein-like DOM at the downstream site in the summer may be an indicator of less "leakiness" of dissolved organic N when autotrophic activity is high or greater assimilation of dissolved organic N by heterotrophs when N is limiting. This lack of organic N result coincides with previous findings of lower N concentrations downstream in summer compared to winter seasons, suggesting that N loading from the adjacent golf course was quickly assimilated by stream primary producers (Gardner and McGlynn, 2009).

In autumn 2016, DOM had higher H/C and O/C ratios compared to summer 2015 (Fig. S11). In general, $C_cH_hO_o$, $C_cH_hO_oS_1$, and $C_cH_hO_oN_1$ composition classes were similar between upstream and downstream sites (Fig. S11). The major differences in chemical composition were greater heterogeneous nature and distinct lignin-like $CHON_2$ chemical species for downstream DOM compared to upstream. The distinct lignin-like $C_cH_hO_oN_2$ composition for downstream DOM is similar to other inland freshwater DOM (Figs. S2-S4) as well as the signatures evident at

the conclusion of the heterotrophic degradation incubation (Fig. S5) (D'Andrilli et al., 2019). We suggest that the accumulation of N_2-containing DOM, perhaps corresponds to algal senescence, local heterotrophic microbial degradation, and greater downstream transport of heterotrophically degraded N-containing algal biomass when organic N is less limiting to secondary production (Fig. 5).

Ecosystem response to N loading may not be detectable in stream DOM quality if lower resolution DOM characterization techniques are used or the input of allochthonous DOM masks the influence of algal production. DOM chemical characterizations using heterogeneous composition percentages from FT-ICR MS and heterogeneous MLB_L calculations may be the key to link DOM composition with ecosystem dynamics like algal growth and senescence. This technique broadens the way we think about aquatic NOM reservoirs and their connective nature instead of evaluating stream sites (or one watershed feature) in isolation. The resolution of DOM composition provided by FT-ICR MS (e.g., allowing focus on biolability of N-containing compounds) may provide a more detailed perspective on metabolism in freshwater ecosystems. In relation to the potential changes in biolability relative to photolability, future work should also incorporate the potential effects of photochemical degradation, which likely occur in streams that have high exposure to direct sunlight (e.g., Cory et al., 2007).

3.3.2. DOM MLB_L in cultivated soils

Both conventional till (FW) and no-till (AW) cropping systems had similar DOM molecular composition (H/C: 0.35 – 2.25 and O/C: 0.05 –
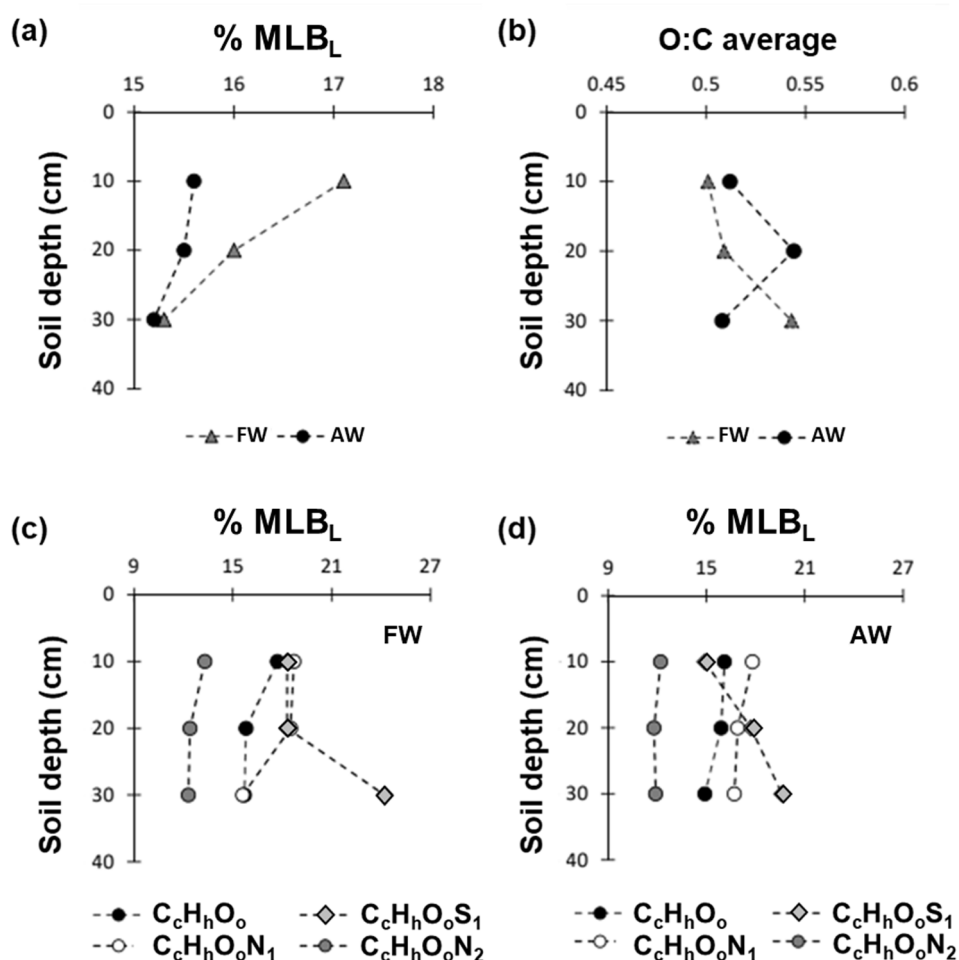

Fig. 6. Dissolved organic matter (DOM) molecular composition metrics of (a) overall MLB_L, (b) oxygen-to-carbon ratio averages, and (c-d) heterogeneous MLB_L from semi-arid arable soils in western Montana of fallow wheat and annual cropping systems across 0–10, 10–20, and 20–30 cm depths; adapted from Romero et al. (2018). FW: fallow wheat from conventional till, AC: annual cropping of no-till wheat. Black and white figure.

0.96) and heterogeneous trends, reflecting terrestrially-derived, lignin-like materials as well as heterotrophic microbial degradation products (Fig. S12 and Table S8). Conventional till FW DOM exhibited higher average MLB_L (16.1 %) relative to no-till AW (15.4 %; Table S8). Conventional till FW was proportionally more biolabile than no-till AW. In previous reports, aromatic-C inputs with lower hydrogen saturation are presumed to be limited by lower shoot-, root-, and rhizodeposit-C being returned to the soil, e.g., 21.1 versus 30.7 Mg ha^{-1} under FW and AW, respectively, (Engel et al., 2017) depleting humic- and tannin-like OM substances (Romero et al., 2017).

Differences in soil organic C between cropping systems may be linked to DOM decomposition pathways with depth. Under conventional till FW, soil OM is expected to be metabolized by soil microbiomes over weeks to months as plowing brings plant-C, i.e., particulate OM, into immediate contact with mineral phases, further disrupting soil aggregates (Chávez-Romero et al., 2016). Crop residues, by contrast, are left on the surface with no-till AW, where plant-C is presumably less available to soil enzymes and microbial populations; as a result, humic-like OM increases (Romero et al., 2017) with particulate OM being gradually incorporated into stable, mineral-associated C pools (Samson et al., 2020; Romero et al., 2021). Among systems, the MLB_L decreased from 17.1 % to 15.2 % within 0–10 and 20–30 cm soil layers, though changes were more pronounced for conventional till FW (Fig. 6a). This shift in MLB_L implied that surface soil layers in both cropping systems contain more hydrogen saturated chemical species available for microbial degradation and that sub-soil OM was enriched by microbially decomposed OM. Oxygenation trends were different for the two systems, with no-till AW increasing in the middle depth (10–20 cm), which could be an indicator of increased microbial degradation (Fig. 6b). Increases in oxygenation were also observed throughout the depth profile for conventional till FW, but much more pronounced at depth (20–30 cm). These findings are consistent with previous paradigms of soil processes throughout vertical profiles (Sanderman et al., 2008; Rumpel and Kogel-Knabner, 2011; Davenport et al., 2023) and represent potential "hot spots" of microbial activity without sun exposure to probe further.

The general distinctions in biolability across these starkly differing tillage and rotational cropping practices were perhaps surprisingly subtle, a finding similar to the subtle general distinctions for the Montana streams along the West Fork of the Gallatin River with known stark differences in algal production (Schade et al., 2010). Therefore, we used the same strategy to extend exploration of DOM biolability to more specific compounds and ecosystem processes (Fig. 6c–d), i.e., using the heterogeneous MLB_L approach (e.g., Fig. 5 inset and Table S8). Hydrogen saturated N-containing compounds were depleted with depth, likely describing microbial degradation *and* biomass building with nutrient availability via N immobilization. All conventional till FW and no-till AW DOM molecular composition trends were the same across $C_cH_hO_o$ and $C_cH_hO_oN_{1-2}$, but not for $C_cH_hO_oS_1$ species (Fig. 6). The marked increase in MLB_L for $C_cH_hO_oS_1$ with depth may suggest that DOM species containing biolabile S-amino acids were not a dominant contributor of sub-soil DOM cycling (Romero et al., 2018). Like the Montana stream study, subtle MLB_L differences represent opportunities to further explore relationships and ecosystem processes. Next steps may include exploring bacterial cell abundances and metabolic pathways given that C and N dynamics from different cropping systems play a role with depth and are largely dominated by microbial mineralization.

3.4. Synthesis and next steps

In analyzing the combined data, we determined multiple strengths of the MLB approach extending beyond sample-to-sample comparisons to tracking DOM compositional changes with unique processes and understanding environmental drivers of C cycling. Through the lens of the MLB_L perspective of DOM from diverse ecosystems, we broaden the information gained from FT-ICR MS data and take our next steps with the MLB approach. The laboratory controlled heterotrophic microbial degradation results set the foundation to better interpret the DOM data from field sample comparisons, the photo-processing experiments helped us rethink what the MLB_R category represents, and the thermal decomposition results shed light on changes in DOM composition with temperature useful for C recycling. The relative changes in MLB_L of a given sampling/field site through a day, season, or year may also help us evaluate the relationships between DOM chemistry and ecosystem processes. For example, increases in MLB_L may correspond to more biologically reactive materials produced by autotrophy, photochemical degradation, enzymatic degradation, and/or transport into an ecosystem. Decreases in MLB_L may relate to the use of biolabile materials by heterotrophs (heterotrophy > autotrophy), the transport of biolabile material downstream, and/or the increase of refractory material into the ecosystem (allochthony > autochthony).

The use of heterogenous MLB_L played a major role to interpret the DOM of the West Fork of the Gallatin River stream samples and Montana soil samples. These two sample sets represented good examples of data that required further analyses of the MLB_L category to evaluate the relationships between DOM chemistry and ecosystem processes. Building on the information gained from the heterotrophic degradation experiment, we used N-containing chemical species to identify "stoichiometrically biolabile" DOM to indicate ecological processes such as, biomass growth and in-situ degradation. Isolating the biolability of heterogeneous DOM provides a deeper understanding to the dynamics of OM composition as influenced by environmental processes.

Originally, the MLB application to FT-ICR MS data defined a zero-slope at H/C = 1.5, though biolability gradients may exist across O/C ratios above the MLB (D'Andrilli et al., 2015). Below that threshold, DOM composition was referred to as 'recalcitrant', i.e., MLB_R, a category defined with respect to microbial degradation. However, reconsideration to include DOM composition transformations with photo-processing opened the door to rethinking what the MLB_R category represented. It raised the question, "What was meant by recalcitrant?" To answer this question, we scrutinized the petroleum OM composition photo-processing data set. Chemically, we know that photo-processing affects aromatic DOM of low hydrogen saturation and reported increases in MLB_L for photo-processed oils. Indeed, the original definition of the MLB_L category did not account for abiotic photochemical lability or photolability, thus the label of 'MLB_L' may be misleading outside the biological context. In general, the term "lability" is confusing due to various temporal and process-specific definitions among scientific disciplines. It is important to define lability in terms of the processes responsible for OM composition changes. Additionally, the MLB does not split a van Krevelen diagram into portions where the use or absence of one MLB_L molecular formula would equate to one formula produced in the MLB_R region. Therefore, we redefine the terms MLB_L and MLB_R to be more specific to biotic and abiotic processes. MLB_L refers to materials that are biolabile from the perspective of heterotrophs and autotrophs, and now includes the end-products of photodegradation as well as material susceptible to thermal degradation. The defined recalcitrant category, MLB_R, now refers to material that may be photolabile, potentially unchanged through biotic and abiotic processes, as well as the end-products of material degraded by heterotrophic microbes. This improvement allows more in-depth DOM chemical understanding and can be used for targeted approaches to FT-ICR MS analysis.

4. Conclusions

Analyzing FT-ICR MS DOM data using the MLB approach is especially useful to reduce the hyper-dimensionality of large, complex DOM data into more digestible packets of information that can be immediately linked to understanding C cycling in different ecosystems. Environments are influenced differently by allochthonous and autochthonous contributions arising from biotic and abiotic processes and diverse transport mechanisms. That complexity clearly demonstrates the value in visualizing DOM dynamics on successive van

Krevelen diagrams; patterns of molecular composition showcasing newly produced, intermediate, and end-product materials. Based on our synthesis across diverse systems and isolated processes, we suggest that the MLB approach should be reframed as a lability index for biotic, thermal, and photochemical processes. With the new understandings of the MLB_L and MLB_R regions, we can begin to think about multiple reactions and potential reaction feedbacks among biological, chemical, and physical processes. Furthermore, we suggested the MLB approach applied to subsets of compound classes may show promise where more specific processes are being investigated.

Over the past few decades, studies have developed DOM metrics and models to better interpret FT-ICR MS molecular data to highlight molecular formula changes with specific environmental processes. Various recent studies have extended what can be understood from DOM chemistry at the molecular level and are important contributions to the organic geochemistry, environmental science, and technology communities. We note that advancing the field of FT-ICR MS DOM characterization is not limited to field and laboratory surveys, but also should include new applications of existing datasets and synthesis to advance DOM science. The updated MLB application affords a useful metric to rank reactive DOM from diverse ecosystems with varying environmental influences and helps us to develop a better understanding of DOM compositional changes with abiotic and biotic processing mechanisms. With the reevaluated MLB approach, the bio- and photo-lability of DOM are distinguishable across diverse applications, mechanisms of C cycling may be inferred from diverse ecosystems, and more generalizable insights may be gained from a single FT-ICR mass spectrum.

Declaration of Competing Interest

The authors declare that they have no known competing financial interests or personal relationships that could have appeared to influence the work reported in this paper.

Data availability

FT-ICR MS data is available on Open Science Framework (osf.io) with the following identifiers: DOI 10.17605/OSF.IO/3YSGD and DOI 10.17605/OSF.IO/UPBWE.

Acknowledgement

Appendix A. Supplementary data

Supplementary data to this article can be found online at https://doi.org/10.1016/j.orggeochem.2023.104667.

References

Avneri-Katz, S., Young, R.B., McKenna, A.M., Chen, H., Corilo, Y.E., Polubesova, T., Borch, T., Chefetz, B., 2017. Adsorptive fractionation of dissolved organic matter (DOM) by mineral soil: Macroscale approach and molecular insight. Organic Geochemistry 103, 113–124.

Bay, R.R., 1967. Ground Water and Vegetation in Two Peat Bogs in Northern Minnesota. Ecology 48, 308–310.

Blakney, G.T., Hendrickson, C.L., Marshall, A.G., 2011. Predator data station: A fast data acquisition system for advanced FT-ICR MS experiments. International Journal of Mass Spectrometry 306, 246–252.

Bostick, K.W., Zimmerman, A.R., Wozniak, A.S., Mitra, S., Hatcher, P.G., 2018. Production and Composition of Pyrogenic Dissolved Organic Matter From a Logical Series of Laboratory-Generated Chars. Frontiers in Earth Science 6.

Bostick, K.W., Zimmerman, A.R., Goranov, A.I., Mitra, S., Hatcher, P.G., Wozniak, A.S., 2020. Photolability of pyrogenic dissolved organic matter from a thermal series of laboratory-prepared chars. Science of the Total Environment 724, 138198.

Brown, T.L., Rice, J.A., 2000. Effect of experimental parameters on the ESI FT-ICR mass spectrum of fulvic acid. Analytical Chemistry 72, 384–390.

Chávez-Romero, Y., Navarro-Noya, Y.E., Reynoso-Martínez, S.C., Sarria-Guzmán, Y., Govaerts, B., Verhulst, N., Dendooven, L., Luna-Guido, M., 2016. 16S metagenomics reveals changes in the soil bacterial community driven by soil organic C, N-fertilizer and tillage-crop residue management. Soil and Tillage Research 159, 1–8.

Chin, Y.-P., McKnight, D.M., D'Andrilli, J., Brooks, N., Cawley, K., Guerard, J., Perdue, E. M., Stedmon, C.A., Tratnyek, P.G., Westerhoff, P., Wozniak, A.S., Bloom, P.R., Foreman, C., Gabor, R., Hamdi, J., Hanson, B., Hozalski, R.M., Kellerman, A., McKay, G., Silverman, V., Spencer, R.G.M., Ward, C., Xin, D., Rosario-Ortiz, F., Remucal, C.K., Reckhow, D., 2023. Identification of next-generation International Humic Substances Society reference materials for advancing the understanding of the role of natural organic matter in the Anthropocene. Aquatic Sciences 85, 32.

Chipman, L., Podgorski, D., Green, S., Kostka, J., Cooper, W., Huettel, M., 2010. Decomposition of plankton-derived dissolved organic matter in permeable coastal sediments. Limnology and Oceanography 55, 857–871.

Comisarow, M.B., Marshall, A.G., 1974. Fourier-Transform Ion-Cyclotron Resonance Spectroscopy. Chemical Physics Letters 25, 282–283.

Cooper, W.T., Chanton, J.C., D'Andrilli, J., Hodgkins, S.B., Podgorski, D.C., Stenson, A. C., Tfaily, M.M., Wilson, R.M., 2022. A History of Molecular Level Analysis of Natural Organic Matter by FTICR Mass Spectrometry and The Paradigm Shift in Organic Geochemistry. Mass Spectrometry Reviews 41, 215–239.

Corilo, Y., 2014. PetroOrg software. Florida State University, Omics LLC, Tallahassee, FL.

Cory, R.M., McKnight, D.M., Chin, Y.-P., Miller, P., Jaros, C.L., 2007. Chemical characteristics of fulvic acids from Arctic surface waters: Microbial contributions and photochemical transformations. Journal of Geophysical Research: Biogeosciences 112, G04S51.

Coward, E.K., Ohno, T., Plante, A.F., 2018. Adsorption and Molecular Fractionation of Dissolved Organic Matter on Iron-Bearing Mineral Matrices of Varying Crystallinity. Environmental Science & Technology 52, 1036–1044.

D'Andrilli, J., Chanton, J.P., Glaser, P.H., Cooper, W.T., 2010. Characterization of dissolved organic matter in northern peatland soil porewaters by ultra high resolution mass spectrometry. Organic Geochemistry 41, 791–799.

D'Andrilli, J., Dittmar, T., Koch, B.P., Purcell, J.M., Marshall, A.G., Cooper, W.T., 2010. Comprehensive characterization of marine dissolved organic matter by Fourier transform ion cyclotron resonance mass spectrometry with electrospray and atmospheric pressure photoionization. Rapid Communications in Mass Spectrometry 24, 643–650.

D'Andrilli, J., Foreman, C.M., Marshall, A.G., McKnight, D.M., 2013. Characterization of IHSS Pony Lake fulvic acid dissolved organic matter by electrospray ionization Fourier transform ion cyclotron resonance mass spectrometry and fluorescence spectroscopy. Organic Geochemistry 65, 19–28.

D'Andrilli, J., Cooper, W.T., Foreman, C.M., Marshall, A.G., 2015. An ultrahigh-resolution mass spectrometry index to estimate natural organic matter lability. Rapid Communications in Mass Spectrometry 29, 2385–2401.

D'Andrilli, J., Smith, H.J., Dieser, M., Foreman, C.M., 2017. Climate driven carbon and microbial signatures through the last ice age. Geochemical Perspectives Letters 4, 29–34.

D'Andrilli, J., Junker, J.R., Smith, H.J., Scholl, E.A., Foreman, C.M., 2019. DOM composition alters ecosystem function during microbial processing of isolated sources. Biogeochemistry 142, 281–298.

D'Andrilli, J., Fischer, S.J., Rosario-Ortiz, F.L., 2020. Advancing Critical Applications of High Resolution Mass Spectrometry for DOM Assessments: Re-Engaging with Mass Spectral Principles, Limitations, and Data Analysis. Environmental Science & Technology 54, 11654–11656.

Davenport, R., Bowen, B.P., Lynch, L.M., Kosina, S.M., Shabtai, I., Northen, T.R., Lehmann, J., 2023. Decomposition decreases molecular diversity and ecosystem similarity of soil organic matter. Proceedings of the National Academy of Sciences USA 120 e2303335120.

Dittmar, T., Koch, B., Hertkorn, N., Kattner, G., 2008. A simple and efficient method for the solid-phase extraction of dissolved organic matter (SPE-DOM) from seawater. Limnology and Oceanography: Methods 6, 230–235.

Dyson, J.L., 1948. Shrinkage of Sperry and Grinnell Glaciers, Glacier National Park, Montana. Geographical Reviews 38, 95–103.

Emmett, M.R., White, F.M., Hendrickson, C.L., Shi, S.D., Marshall, A.G., 1998. Application of micro-electrospray liquid chromatography techniques to FT-ICR MS to enable high-sensitivity biological analysis. Journal of the American Society for Mass Spectrometry 9, 333–340.

Engel, R.E., Miller, P.R., McConkey, B.G., Wallander, R., 2017. Soil Organic Carbon Changes to Increasing Cropping Intensity and No-Till in a Semiarid Climate. Soil Science Society of America Journal 81, 404–413.

Gardner, K.K., McGlynn, B.L., 2009. Seasonality in spatial variability and influence of land use/land cover and watershed characteristics on stream water nitrate concentrations in a developing watershed in the Rocky Mountain West. Water Resources Research 45, W08411.

Gardner, K.K., McGlynn, B.L., Marshall, L.A., 2011. Quantifying watershed sensitivity to spatially variable N loading and the relative importance of watershed N retention mechanisms. Water Resources Research 47, W08524.

Glaser, P.H., Wheeler, G.A., Gorham, E., Wright, H.E., 1981. The Patterned Mires of the Red Lake Peatland, Northern Minnesota - Vegetation, Water Chemistry and Landforms. Journal of Ecology 69, 575–599.

Gonsior, M., Peake, B.M., Cooper, W.T., Podgorski, D., D'Andrilli, J., Cooper, W.J., 2009. Photochemically induced changes in dissolved organic matter identified by ultrahigh resolution fourier transform ion cyclotron resonance mass spectrometry. Environmental Science & Technology 43, 698–703.

Goranov, A.I., Wozniak, A.S., Bostick, K.W., Zimmerman, A.R., Mitra, S., Hatcher, P.G., 2020. Photochemistry after fire: Structural transformations of pyrogenic dissolved organic matter elucidated by advanced analytical techniques. Geochimica Et Cosmochimica Acta 290, 271–292.

Hawkes, J.A., D'Andrilli, J., Agar, J.N., Barrow, M.P., Berg, S.M., Catalán, N., Chen, H., Chu, R.K., Cole, R.B., Dittmar, T., Gavard, R., Gleixner, G., Hatcher, P.G., He, C., Hess, N.J., Hutchins, R.H.S., Ijaz, A., Jones, H.E., Kew, W., Khaksari, M., Palacio Lozano, D.C., Lv, J., Mazzoleni, L.R., Noriega-Ortega, B.E., Osterholz, H., Radoman, N., Remucal, C.K., Schmitt, N.D., Schum, S.K., Shi, Q., Simon, C., Singer, G., Sleighter, R.L., Stubbins, A., Thomas, M.J., Tolic, N., Zhang, S., Zito, P., Podgorski, D.C., 2020. An international laboratory comparison of dissolved organic matter composition by high resolution mass spectrometry: Are we getting the same answer? Limnology and Oceanography: Methods 18, 235–258.

Heinselman, M.L., 1963. Forest Sites, Bog Processes, and Peatland Types in the Glacial Lake Agassiz Region, Minnesota. Ecological Monographs 33, 327–374.

Hertkorn, N., Benner, R., Frommberger, M., Schmitt-Kopplin, P., Witt, M., Kaiser, K., Kettrup, A., Hedges, J.I., 2006. Characterization of a major refractory component of marine dissolved organic matter. Geochimica Et Cosmochimica Acta 70, 2990–3010.

Hughey, C.A., Rodgers, R.P., Marshall, A.G., 2002. Resolution of 11,000 compositionally distinct components in a single electrospray ionization Fourier transform ion cyclotron resonance mass spectrum of crude oil. Analytical Chemistry 74, 4145–4149.

Kaiser, N.K., Quinn, J.P., Blakney, G.T., Hendrickson, C.L., Marshall, A.G., 2011. A novel 9.4 tesla FTICR mass spectrometer with improved sensitivity, mass resolution, and mass range. Journal of the American Society for Mass Spectrometry 22, 1343–1351.

Kim, S., Kramer, R.W., Hatcher, P.G., 2003. Graphical method for analysis of ultrahigh-resolution broadband mass spectra of natural organic matter, the van Krevelen diagram. Analytical Chemistry 75, 5336–5344.

King, S.M., Leaf, P.A., Olson, A.C., Ray, P.Z., Tarr, M.A., 2014. Photolytic and photocatalytic degradation of surface oil from the Deepwater Horizon spill. Chemosphere 95, 415–422.

King, A.C.F., Thomas, E.R., Pedro, J.B., Markle, B., Potocki, M., Jackson, S.L., Wolff, E., Kalberer, M., 2019. Organic Compounds in a Sub-Antarctic Ice Core: A Potential Suite of Sea Ice Markers. Geophysical Research Letters 46, 9930–9939.

Koch, B.P., Dittmar, T., 2006. From mass to structure: an aromaticity index for high-resolution mass data of natural organic matter. Rapid Communications in Mass Spectrometry 20, 926–932.

Krajewski, L.C., Rodgers, R.P., Marshall, A.G., 2017. 126 264 Assigned Chemical Formulas from an Atmospheric Pressure Photoionization 9.4 T Fourier Transform Positive Ion Cyclotron Resonance Mass Spectrum. Analytical Chemistry 89, 11318–11324.

Kujawinski, E.B., Hatcher, P.G., Freitas, M.A., 2002. High-resolution Fourier transform ion cyclotron resonance mass spectrometry of humic and fulvic acids: improvements and comparisons. Analytical Chemistry 74, 413–419.

Kujawinski, E.B., Del Vecchio, R., Blough, N.V., Klein, G.C., Marshall, A.G., 2004. Probing molecular-level transformations of dissolved organic matter: insights on

photochemical degradation and protozoan modification of DOM from electrospray ionization Fourier transform ion cyclotron resonance mass spectrometry. Marine Chemistry 92, 23–37.

LaBrie, R., Péquin, B., Fortin St-Gelais, N., Yashayaev, I., Cherrier, J., Gélinas, Y., Guillemette, F., Podgorski, D.C., Spencer, R.G.M., Tremblay, L., Maranger, R., 2022. Deep ocean microbial communities produce more stable dissolved organic matter through the succession of rare prokaryotes. Science Advances 8, eabn0035.

Lemkau, K.L., Peacock, E.E., Nelson, R.K., Ventura, G.T., Kovecses, J.L., Reddy, C.M., 2010. The M/V Cosco Busan spill: source identification and short-term fate. Marine Pollution Bulletin 60, 2123–2129.

Limbach, P.A., Schweikhard, L., Cowen, K.A., Mcdermott, M.T., Marshall, A.G., Coe, J.V., 1991. Observation of the Doubly Charged, Gas-Phase Fullerene Anions C_{60}^{2-} and C_{70}^{2-}. Journal of the American Chemical Society 113, 6795–6798.

Logue, J.B., Stedmon, C.A., Kellerman, A.M., Nielsen, N.J., Andersson, A.F., Laudon, H., Lindstrom, E.S., Kritzberg, E.S., 2016. Experimental insights into the importance of aquatic bacterial community composition to the degradation of dissolved organic matter. The ISME Journal 10, 533–545.

Marshall, A.G., Verdun, F.R., 1990. Fourier Transforms in NMR, Optical, and Mass Spectrometry: A User's Handbook. Elsevier, Amsterdam.

Masiello, C.A., 2004. New directions in black carbon organic geochemistry. Marine Chemistry 92, 201–213.

Minor, E.C., Swenson, M.M., Mattson, B.M., Oyler, A.R., 2014. Structural characterization of dissolved organic matter: a review of current techniques for isolation and analysis. Environmental Science-Processes & Impacts 16, 2064–2079.

Mopper, K., Stubbins, A., Ritchie, J.D., Bialk, H.M., Hatcher, P.G., 2007. Advanced instrumental approaches for characterization of marine dissolved organic matter: extraction techniques, mass spectrometry, and nuclear magnetic resonance spectroscopy. Chemical Reviews 107, 419–442.

Mukherjee, A., Zimmerman, A.R., Harris, W., 2011. Surface chemistry variations among a series of laboratory-produced biochars. Geoderma 163, 247–255.

Podgorski, D.C., Hamdan, R., McKenna, A.M., Nyadong, L., Rodgers, R.P., Marshall, A.G., Cooper, W.T., 2012. Characterization of pyrogenic black carbon by desorption atmospheric pressure photoionization Fourier transform ion cyclotron resonance mass spectrometry. Analytical Chemistry 84, 1281–1287.

Purcell, J.M., Juyal, P., Kim, D.G., Rodgers, R.P., Hendrickson, C.L., Marshall, A.G., 2007. Sulfur speciation in petroleum: Atmospheric pressure photoionization or chemical derivatization and electrospray ionization fourier transform ion cyclotron resonance mass spectrometry. Energy & Fuels 21, 2869–2874.

Ray, P.Z., Chen, H., Podgorski, D.C., McKenna, A.M., Tarr, M.A., 2014. Sunlight creates oxygenated species in water-soluble fractions of Deepwater Horizon oil. Journal of Hazardous Materials 280, 636–643.

Roebuck, J.A., Podgorksi, D.C., Wagner, S., Jaffe, R., 2017. Photodissolution of charcoal and fire-impacted soil as a potential source of dissolved black carbon in aquatic environments. Organic Geochemistry 112, 16–21.

Romero, C.M., Engel, R.E., D'Andrilli, J., Chen, C.C., Zabinski, C., Miller, P.R., Wallander, R., 2017. Bulk optical characterization of dissolved organic matter from semiarid wheat-based cropping systems. Geoderma 306, 40–49.

Romero, C.M., Engel, R.E., D'Andrilli, J., Chen, C.C., Zabinski, C., Miller, P.R., Wallander, R., 2018. Patterns of change in permanganate oxidizable soil organic matter from semiarid drylands reflected by absorbance spectroscopy and Fourier transform ion cyclotron resonance mass spectrometry. Organic Geochemistry 120, 19–30.

Romero, C.M., Hao, X.Y., Hazendonk, P., Schwinghamer, T., Chantigny, M., Fonteyne, S., Verhulst, N., 2021. Tillage-residues affect mineral-associated organic matter on Vertisols in northern Mexico. Geoderma Regional 27, e00430.

Rumpel, C., Kogel-Knabner, I., 2011. Deep soil organic matter-a key but poorly understood component of terrestrial C cycle. Plant and Soil 338, 143–158.

Samson, M.E., Chantigny, M.H., Vanasse, A., Menasseri-Aubry, S., Angers, D.A., 2020. Coarse mineral-associated organic matter is a pivotal fraction for SOM formation and is sensitive to the quality of organic inputs. Soil Biology and Biochemistry 149, 107935.

Sanderman, J., Baldock, J.A., Amundson, R., 2008. Dissolved organic carbon chemistry and dynamics in contrasting forest and grassland soils. Biogeochemistry 89, 181–198.

Savory, J.J., Kaiser, N.K., McKenna, A.M., Xian, F., Blakney, G.T., Rodgers, R.P., Hendrickson, C.L., Marshall, A.G., 2011. Parts-per-billion Fourier transform ion cyclotron resonance mass measurement accuracy with a "walking" calibration equation. Analytical Chemistry 83, 1732–1736.

Schade, P., Kusnierz, L., Gardner, K.K., McGlynn, B.L., Marshall, L., 2010. The West Fork Gallatin River Watershed Total Maximum Daily Loads (TMDLS) and Framework Watershed Water Quality Improvement Plan. Report. Montana Department of Environmental Quality.

Schneider, M., Hilf, M.D., Vogt, U., Schmidt, M., 2010. The benzene polycarboxylic acid (BPCA) pattern of wood pyrolyzed between 200 °C and 1000 °C. Organic Geochemistry 41, 1082–1088.

Sebestyen, S.D., Dorrance, C., Olson, D.M., Verry, E.S., Kolka, R.K., Elling, A.E., Kyllander, R.L., 2011. Long-term monitoring sites and trends at the Marcell Experimental Forest. In: Kolka, R.K., Sebestyen, S.D., Verry, E.S., Brooks, K.N. (Eds.), Peatland Biogeochemistry and Watershed Hydrology at the Marcell Experimental Forest. CRC Press, Boca Raton, FL, pp. 15–71.

Sebestyen, S.D., Lany, N.K., Roman, D.T., Burdick, J.M., Kyllander, R.L., Verry, E.S., Kolka, R.K., 2021. Hydrological and meteorological data from research catchments at the Marcell Experimental Forest, Minnesota, USA. Hydrological Processes 35, e14092.

Sleighter, R.L., Hatcher, P.G., 2008. Molecular characterization of dissolved organic matter (DOM) along a river to ocean transect of the lower Chesapeake Bay by

ultrahigh resolution electrospray ionization Fourier transform ion cyclotron resonance mass spectrometry. Marine Chemistry 110, 140–152.

Smith, H.J., Tigges, M., D'Andrilli, J., Parker, A., Bothner, B., Foreman, C.M., 2018. Dynamic processing of DOM: Insight from exometabolomics, fluorescence spectroscopy, and mass spectrometry. Limnology and Oceanography Letters 3, 225–235.

Stenson, A.C., Marshall, A.G., Cooper, W.T., 2003. Exact masses and chemical formulas of individual Suwannee River fulvic acids from ultrahigh resolution electrospray ionization Fourier transform ion cyclotron resonance mass spectra. Analytical Chemistry 75, 1275–1284.

Stubbins, A., Spencer, R.G.M., Chen, H.M., Hatcher, P.G., Mopper, K., Hernes, P.J., Mwamba, V.L., Mangangu, A.M., Wabakanghanzi, J.N., Six, J., 2010. Illuminated darkness: Molecular signatures of Congo River dissolved organic matter and its photochemical alteration as revealed by ultrahigh precision mass spectrometry. Limnology and Oceanography 55, 1467–1477.

Tanaka, D.L., Lyon, D.J., Miller, P.R., Merrill, S.D., McConkey, B.G., 2010. Soil and Water Conservation Advances in the Semiarid Northern Great Plains. In: Zobeck, T.M., Schillinger, W.F. (Eds.), Soil and Water Conservation Advances in the United States. SSSA Special Publications, pp. 81–102.

Tfaily, M.M., Hamdan, R., Corbett, J.E., Chanton, J.P., Glaser, P.H., Cooper, W.T., 2013. Investigating dissolved organic matter decomposition in northern peatlands using complimentary analytical techniques. Geochimica Et Cosmochimica Acta 112, 116–129.

Wagner, S., Jaffé, R., Stubbins, A., 2018. Dissolved black carbon in aquatic ecosystems. Limnology and Oceanography Letters 3, 168–185.

Wang, Y., Xie, R., Shen, Y., Cai, R., He, C., Chen, Q., Guo, W., Shi, Q., Jiao, N., Zheng, Q., 2022. Linking Microbial Population Succession and DOM Molecular Changes in Synechococcus-Derived Organic Matter Addition Incubation. Microbiology Spectrum 10, e02308.

Ward, C.P., Nalven, S.G., Crump, B.C., Kling, G.W., Cory, R.M., 2017. Photochemical alteration of organic carbon draining permafrost soils shifts microbial metabolic pathways and stimulates respiration. Nature Communications 8, 772.

Wozniak, A.S., Goranov, A.I., Mitra, S., Bostick, K.W., Zimmerman, A.R., Schlesinger, D. R., Myneni, S., Hatcher, P.G., 2020. Molecular heterogeneity in pyrogenic dissolved organic matter from a thermal series of oak and grass chars. Organic Geochemistry 148, 104065.

Wright, H.E., 1972. A Quaternary history of Minnesota. In: Sims, P.K., Morey, G.B. (Eds.), Geology of Minnesota: A Centennial Volume. Minnesota Geological Survey, Saint Paul, MN, pp. 515–592.

Zhen, Y., Xiaoming, L., Changya, C., Hanpeng, L., Zhi, C., Shungui, Z., 2019. Molecular insights into the transformation of dissolved organic matter during hyperthermophilic composting using ESI FT-ICR MS. Bioresource Technology 292, 122007.

Zimmerman, A.R., 2010. Abiotic and microbial oxidation of laboratory-produced black carbon (biochar). Environmental Science & Technology 44, 1295–1301.

Zito, P., Podgorski, D.C., Johnson, J., Chen, H., Rodgers, R.P., Guillemette, F., Kellerman, A.M., Spencer, R.G.M., Tarr, M.A., 2019. Molecular-Level Composition and Acute Toxicity of Photosolubilized Petrogenic Carbon. Environmental Science & Technology 53, 8235–8243.

Zito, P., Podgorski, D.C., Bartges, T., Guillemette, F., Roebuck, J.A., Spencer, R.G.M., Rodgers, R.P., Tarr, M.A., 2020. Sunlight-Induced Molecular Progression of Oil into Oxidized Oil Soluble Species, Interfacial Material, and Dissolved Organic Matter. Energy & Fuels 34, 4721–4726.